Hindawi Publishing Corporation
Advances in High Energy Physics
Volume 2012, Article ID 235686, 34 pages
doi:10.1155/2012/235686

*Review Article*

# Geoneutrinos

**Ondřej Šrámek,[1] William F. McDonough,[1] and John G. Learned[2]**

[1] *Department of Geology, University of Maryland, College Park, MD 20742, USA*
[2] *Department of Physics and Astronomy, University of Hawaii, Honolulu, HI 96822, USA*

Correspondence should be addressed to Ondřej Šrámek, sramek@umd.edu

Received 9 July 2012; Accepted 20 October 2012

Academic Editor: Arthur B. McDonald



Neutrino geophysics is an emerging interdisciplinary field with the potential to map the abundances and distribution of radiogenic heat sources in the continental crust and deep Earth. To date, data from two different experiments quantify the amount of Th and U in the Earth and begin to put constraints on radiogenic power in the Earth available for driving mantle convection and plate tectonics. New improved detectors are under construction or in planning stages. Critical testing of compositional models of the Earth requires integrating geoneutrino and geological observations. Such tests will lead to significant constraints on the absolute and relative abundances of U and Th in the continents. High radioactivity in continental crust puts limits on land-based observatories' capacity to resolve mantle models with current detection methods. Multiple-site measurement in oceanic areas away from continental crust and nuclear reactors offers the best potential to extract mantle information. Geophysics would benefit from directional detection and the detectability of electron antineutrinos from potassium decay.

## 1. Introduction

In the simplest view, the Earth formed hot and has been cooling since [1]. The initial hot state 4.5 billion years ago was a result of gravitational energy of accretion and global differentiation largely released as heat. As a first-order estimate, the gravitational energy $GM^2/R$ released by accumulating the Earth of mass $M$ and radius $R$ from spatially dispersed building blocks is enough to increase the temperature by tens of thousands of Kelvin [2] if entirely converted to heat. Further heat is released upon differentiation and gravitational segregation of the metallic core from the overlying silicate shell and possibly also provided by short-lived radioactivity. Compared to melting temperatures of silicates and metal that make up the Earth ($\lesssim$2000 K), these observations suggest an early period of large-scale melting.

In 1862, William Thomson, future Lord Kelvin, communicated his now famous estimate of Earth's age [3]. Assuming conductive cooling of an initially molten Earth, and

**Table 1:** Terminology used in the paper.

| | |
|---|---|
| BSE | Bulk silicate Earth |
| CC | Continental crust |
| CL | Confidence level |
| CMB | Core-mantle boundary |
| DM | Depleted mantle |
| HPE | Heat producing elements |
| LLSVPs | Large low shear-wave velocity provinces |
| MORB | Mid-ocean ridge basalt |
| TNU | Terrestrial neutrino unit |
| ULVZs | Ultra-low velocity zones |

using best existing estimates of rock melting temperature, subsurface temperature gradient, and thermal conductivity, he arrived at age of 98 My, allowing for a span between 20 and 400 My. Kelvin later downgraded his estimate to 20–40 My [4]. (More on the interesting subject of Earth's age determination in [5, 6].) We now understand the reasons why Kelvin's calculation underestimated the age of the Earth by two orders of magnitude: an internal source of heat is provided by long-lived radioactivity [7] and, more importantly, thermal diffusion is not the primary process of controlling heat loss from the Earth's interior [8].

Constraining Earth's thermal history is a major task of geophysics. It requires knowledge of the present-day thermal state, the energy sources available for the planet, and the processes that operate over time. Uncertainties remain, even if great progress has been made, especially in the last several decades since the acceptance of the plate tectonics paradigm in the 1970s [9]. The progress was made possible thanks to advances in geophysical observations, chemical analyses of rock samples, laboratory experiments on Earth constituents, and understanding of Earth's internal dynamics based on theoretical arguments and numerical modeling. Current understanding of Earth's thermal evolution appreciates the dominant role of advective transport of heat by large-scale convection in large part of Earth's interior. Knowledge of present-day thermal state is limited by uncertainties in abundances of heat-producing elements (HPEs; Table 1 explains abbreviations used in this paper), long-lived radioactive isotopes of U, Th, and K. Distribution of the HPEs within the Earth volume must be known as well.

Geoscience is a broadly interdisciplinary field and now embraces particle physics experiments. The first detection of weakly interacting neutrinos—in fact, nuclear reactor-generated antineutrinos—by Reines and Cowan's research team was confirmed in 1956 [10]. Counting electron antineutrinos generated in $\beta$-decays of HPEs in Earth's interior can provide direct information about the deep-seated radioactivity, not obtainable by any other means. Measurement of Earth's internal radioactivity by terrestrial neutrino detection was first proposed by Eder [11], and the idea was further developed by Marx and coworkers [12–14]. Krauss et al. [15] presented a comprehensive overview of antineutrino geophysics, including emission predictions based on a geological model and discussion of possible detection mechanisms. Raghavan et al. [16] and Rothschild et al. [17] were the first to examine the potential of KamLAND and Borexino detectors for geoneutrino measurement. Experimental efforts resulted in the first geoneutrino detections by KamLAND [18, 19] and Borexino [20], which begin to answer relevant geophysical questions. New geoneutrino detectors are being developed: SNO+ [21] is scheduled to go online in 2013, and several other experiments with geoneutrino detection capabilities have been proposed.

Neutrino physics gains momentum in the geophysical community. Kobayashi and Fukao's 1991 paper [22] marks the first geoneutrino publication in a specialized geophysical journal. Meetings with specific focus on neutrino geophysics took place at University of Hawaii in 2005 [23] and 2007 [24], at SNOLAB in 2008 [25], in Gran Sasso in 2010 [26], and in Deadwood, South Dakota in 2011 [27]. A special session on geoneutrinos was convened at American Geophysical Union 2006 Joint Assembly [28]. Proceedings from the 2005 meeting were collectively published in Volume 99 of Earth, Moon, and Planets (Neutrino Geophysics, Proceedings of Neutrino Sciences 2005, http://link.springer.com/journal/11038/99/1/) and reprinted in a book format [29]. Geoneutrino physics is a subject of Master's [30] and Ph.D. [31] theses, as well as outreach and popular articles aimed at broader scientific community [32–35].

In this paper we focus on the use of neutrinos for geology. Other aspects of neutrino research are covered by other papers throughout this comprehensive issue. Recent review articles on geoneutrinos include Enomoto et al. [36], Fiorentini et al. [37], Dye [38], and Dye [39]. Parts of this paper closely follow the presentation of Dye [39]. The structure of this paper is as follows. We first present the "state of the Earth" in Section 2 and discuss the geophysical motivation for geoneutrino studies. We then review the relevant details of geoneutrino production (Section 3) and oscillation (Section 4), introduce calculation of geoneutrino flux (Section 5), discuss geoneutrino detection (Section 6) and detectors (Section 7), show predictions of geoneutrino flux (Section 8), review geoneutrino observations (Section 9), and discuss future prospects (Section 10).

## 2. Geophysical Questions Driving Geoneutrino Research

Seismic observation combined with gravity data and geochemical inputs inform us about the architecture of the Earth. The first-order internal structure has been known, at least qualitatively, since the 1930s by which time the main domains of the differentiated Earth were identified: the inner core, the outer core, the mantle, and the crust, as shown in Figure 1. The mantle and the crust constitute the silicate Earth, the core is mostly metallic iron.

The rate at which the Earth loses heat is a balance between the secular cooling of the Earth and the radiogenic heat production, which is the only significant heat source. Understanding the relative contributions is important for understanding the Earth's dynamics and evolution over time. The most recent assessment of the present-day energy budget is provided by Mareschal et al. [40]. Detailed discussion of Earth's thermal history can be found in reviews by Jaupart et al. [41], Korenaga [42], and Lay et al. [43].

The Earth's heat loss can be estimated from heat flow measurements supplemented with geophysical modeling in oceanic areas [41, 44–47]. In the latest analysis of surface heat flux, J. H. Davies and D. R. Davies [47] used ~38000 heat flow measurements and geological data. Heat flow on young sea floor is described by half-space cooling model [48] to account for hydrothermal circulation near oceanic spreading centers, which provides advective heat transport mechanism in addition to measurable conducted heat. J. H. Davies and D. R. Davies [47] arrive at total heat loss of $47 \pm 2$ TW, where 16 TW is lost from the continents and 31 TW from oceans. The analysis of Jaupart et al. [41] reports $46 \pm 3$ TW, with 14 TW lost over continental regions. The recent proposition of much lower oceanic heat loss [49] seems untenable [50, 51]. While the heat loss estimates are robust, it has been suggested that present-day heat loss is below the long-term average due to recent slowdown in oceanic spreading rates [52].

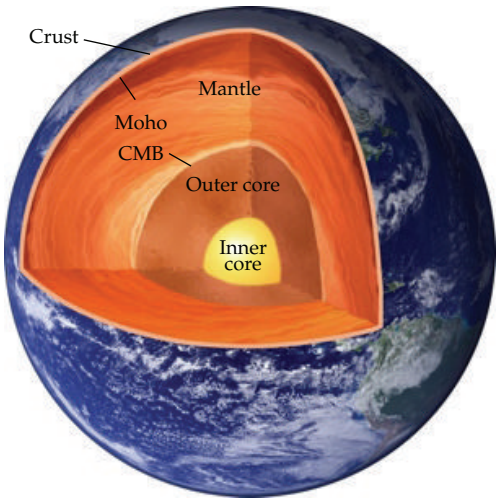


**Figure 1:** Schematic of Earth's internal structure. Adapted from http://tinyurl.com/lblgeonu.

A significant part of heat flux over continents comes from radiogenic heat produced in the continental crust (CC) of average thickness ~40 km. The high abundances of HPEs are a consequence of CC formation that involves repeated melting, a fractionation process which concentrates the so-called incompatible elements (including U, Th, and K) in the melt phase. Generally the crustal concentrations of HPEs are the highest near the surface and decrease downwards by a factor of ten to its base [53]. As we discuss later, this has implications for geoneutrino studies where the signal at continental measurement sites is dominated by locally produced crustal geoneutrinos. The radiogenic heat production in the CC is estimated from crustal compositional models and heat flux analysis and adds to ~8 TW of power [40]. The crustal heat source does not fuel convection in the Earth's mantle and can be subtracted from the total heat loss (~47 TW) to obtain a mantle heat flow of ~39 TW.

Heat supplied by the core to the mantle across the core-mantle boundary (CMB) provides basal heating for mantle convection. In addition to secular cooling of the core, the CMB heat flux includes contributions from the latent heat of crystallization and from the gravitational energy release as the solid inner core grows (the possibility of core radiogenic heating will be discussed shortly) [43]. Estimates of CMB heat flow are largely based on scaling analyses of compositionally driven convection in the molten outer core and are tightly linked to age and evolution of the inner core and the operation of the geodynamo. The uncertainty on the CMB heat flow, with values estimated in the range of 5–15 TW, is large [40, 43, 54].

Rock samples available for direct chemical analysis only come from shallow depths of 100 to 200 km at most. Composition of the uppermost mantle can be inferred from analyses of basalts erupted at midoceanic ridges (i.e., MORBs). Estimation of HPE abundances and distribution in the remainder of Earth interior has to be deduced indirectly. Main points to consider are (i) with how much HPEs did the Earth accrete, (ii) what was the fate of these elements during core formation, a global differentiation (and chemical fractionation) process, and (iii) how did the distribution of HPEs evolve after core formation was completed until present day, especially in the silicate part of the Earth.

**Table 2:** Abundance estimates of U, Th, and K in BSE and DM. Uncertainties are included where available.

| U (ppb) | Th (ppb) | K (ppm) | Th/U | K/U | Power (TW) | Reference |
|---|---|---|---|---|---|---|
| Bulk silicate Earth (BSE) | | | | | | |
| *Collisional erosion model* | | | | | | |
| 10 | 38 | 120 | 3.8 | 12000 | 9.6 | O'Neill and Palme [62] |
| *Based on enstatite chondrites* | | | | | | |
| 13.5 | 41.7 | 385 | 3.1 | 28500 | 15 | Javoy [63] |
| 12.1 | 49.2 | 146 | 3.5 | 12000 | 11 | Javoy et al. [64]† |
| *Based on terrestrial rocks and C1 carbonaceous chondrite ratios of RLE abundances* | | | | | | |
| 20.8 | 79.0 | 264 | 3.8 | 12700 | 20 | Hart and Zindler [58] |
| 20.3 ± 20% | 79.5 ± 15% | 240 ± 20% | 3.9 | 11800 | 20 ± 4 | McDonough and Sun [55] |
| 21.8 ± 15% | 83.4 ± 15% | 260 ± 15% | 3.8 | 11900 | 21 ± 3 | Palme and O'Neill [59] |
| 17.3 ± 3.0 | 62.6 ± 10.7 | 190 ± 40 | 3.6 | 11000 | 16 ± 3 | Lyubetskaya and Korenaga [61] |
| 20 ± 4 | 80 ± 12 | 280 ± 60 | 4.0 | 13800 | 20 ± 4 | Arevalo et al. [60] |
| *Based on energetics of mantle convection ("conventional" scaling)* | | | | | | |
| 31 | 124 | 310 | 4.0 | 10000 | 30 | Turcotte and Schubert [65] |
| Depleted mantle (DM)—MORB source | | | | | | |
| 3.2 ± 0.5 | 7.9 ± 1.1 | 50 | 2.5 | 15600 | 2.8 ± 0.4* | Workman and Hart [66] |
| 4.7 ± 30% | 13.7 ± 30% | 60 ± 28% | 2.9 | 12800 | 4.1 ± 1.2* | Salters and Stracke [67] |
| 8 ± 20% | 22 ± 20% | 152 ± 20% | 2.8 | 19000 | 7.5 ± 1.5* | Arevalo and McDonough [68] |

†Model of Javoy et al. [64] is constructed following Javoy's recipe as described in [69]. *Calculation of radiogenic power for DM estimates assumes that the entire mantle has DM composition.

The first issue is usually addressed by relating the Earth composition in some way to chemical abundances measured in primitive meteorites. One approach consists of using the available rock samples from the crust and shallow mantle to infer the original composition of the primitive (or primordial) mantle prior to crust formation. An additional constraint imposes that the ratios of so-called refractory lithophile elements (RLE) match those of C1 carbonaceous chondrites, the most primitive chondrites whose composition best matches the solar photosphere. The lithophile elements (according to Goldschmidt's classification) are those excluded from the metallic core because during differentiation these elements partition effectively into the silicates and not the sulfides nor metals. The term refractory signifies a high temperature of condensation from the solar nebula. The actual model RLE abundances are ~2.75 times larger relative to the C1 chondrites [55]. Both U and Th are RLEs. Potassium is also lithophile but moderately volatile during accretion, which makes the K abundance estimate particularly difficult. Indeed, the K/U abundance ratio of the Earth is estimated to be some eight times less than that in C1 chondritic meteorites [56]. The affinity of U, Th, and K for silicate phase argues for no radiogenic heat production in the core [57]. HPE abundances in the bulk silicate Earth (BSE, i.e., mantle + crust combined) for several estimates from this class of models are shown in Table 2. The typical radiogenic heat production from these models is ~20 TW in the BSE [55, 58–60], even though a somewhat lower power (~17 TW) was recently proposed [61]. We call this class of estimates "geochemical" BSE models.

An alternative meteorite-based approach toward estimation of bulk Earth composition appreciates the isotopic similarity of enstatite chondrites with terrestrial samples and uses the chondritic abundances at face value [63, 64]. Javoy et al. [64] argue for a BSE composition that produces a mere ~11 TW of radiogenic power (Table 2). We call these

models "cosmochemical" estimates. Other models exist that yield similarly low abundance of the heat producing elements. O'Neill and Palme [62] recently proposed a model whereby the early developed Earth crust, enriched in highly incompatible elements (e.g., U, Th, and K) was stripped off by collisional erosion, which resulted in marked depletions of these elements from the bulk silicate Earth. Consequently, the O'Neill and Palme model has a bulk silicate Earth that contains as little as 10 ppb U, 38 ppb Th and 120 ppm K. In terms of absolute concentration, this is comparable to the Javoy et al. model.

Geodynamical modeling of mantle dynamics provides a different type of constraints on the radiogenic power. Mantle radioactivity is an important energy source that contributes to the power that drives the solid-state convection in the mantle. Tremendous progress has been made over the last fifty years in theoretical understanding as well as numerical modeling of thermal convection in planetary interiors [70, 71]. An important class of Earth's thermal evolution models consider the simple energy balance, where the net heat loss out of the mantle has to reflect a combination of mantle cooling and heat production. The dynamical link between the mantle internal temperature and the heat loss comes from the relation between the vigor of convection and the heat flux. This is known as the Nusselt number-Rayleigh number (Nu-Ra) scaling, which refers to the characteristic dimensionless quantities in convective heat transfer problems. In these so-called parameterized thermal evolution models, the mantle temperature and heat loss can be traced back in time starting from present-day initial conditions. In principle, a smaller power of radiogenic heat sources requires a larger temperature increase (backward in time) in order to account for a given heat flux. Classical parameterized models call for a significant fraction, ~60–80 percent, of present-day mantle heat loss to come from radiogenic heating (this is often referred to as a requirement on the mantle Urey ratio being 0.6–0.8) in order to avoid unrealistically high mantle temperature in Earth's history, in conflict with early rock record [65, 70, 72]. This translates to $\gtrsim$23 TW of mantle radiogenic power or $\gtrsim$30 TW in BSE as required by a "geodynamical" model (Table 2) and is at odds with the geochemical BSE estimates.

It must be pointed out that our high Urey number geodynamical BSE estimate is based on a simple Nu-Ra scaling of the "conventional" parameterized convection models. Another way to avoid the Archean thermal catastrophe is to assume a different scaling law with a weaker coupling between the heat loss and mantle temperature (first suggested by Christensen [73]). A specific mechanism for the modification of the scaling law in early Earth has been proposed [74] (see also [75]). Other solutions invoke the specifics of the Earth-like convection which are not accounted for in the simple scaling [41, 76–80]. These alternative thermal evolution models are motivated by the geochemical constraint on HPE abundances (i.e., low mantle Urey ratio, ~0.3). Overall there is a large variance in Urey number predictions from geodynamical models of different degrees of sophistication. We use the conventional scaling as a high estimate for the HPE abundances in the Earth.

The discussion of BSE composition shows that there are three competing estimates—cosmochemical (poor in HPE), geochemical (intermediate), and geodynamical (rich). Figure 2 shows the temporal evolution of available radiogenic power throughout Earth's history as predicted by the three models. The breakdown of the heating contributed by the four radionuclides is also shown, and somewhat differs between the cosmochemical [64] and geochemical [60] estimates because of differences in Th/U and K/U ratios. At present, about 80% of radiogenic powers is supplied in roughly equal measure by $^{238}$U and $^{232}$Th, the remaining 20% being provided by $^{40}$K; present-day $^{235}$U contribution is below 2% of total power. Heating by $^{40}$K and $^{235}$U, however, dominated in the planet's early history.

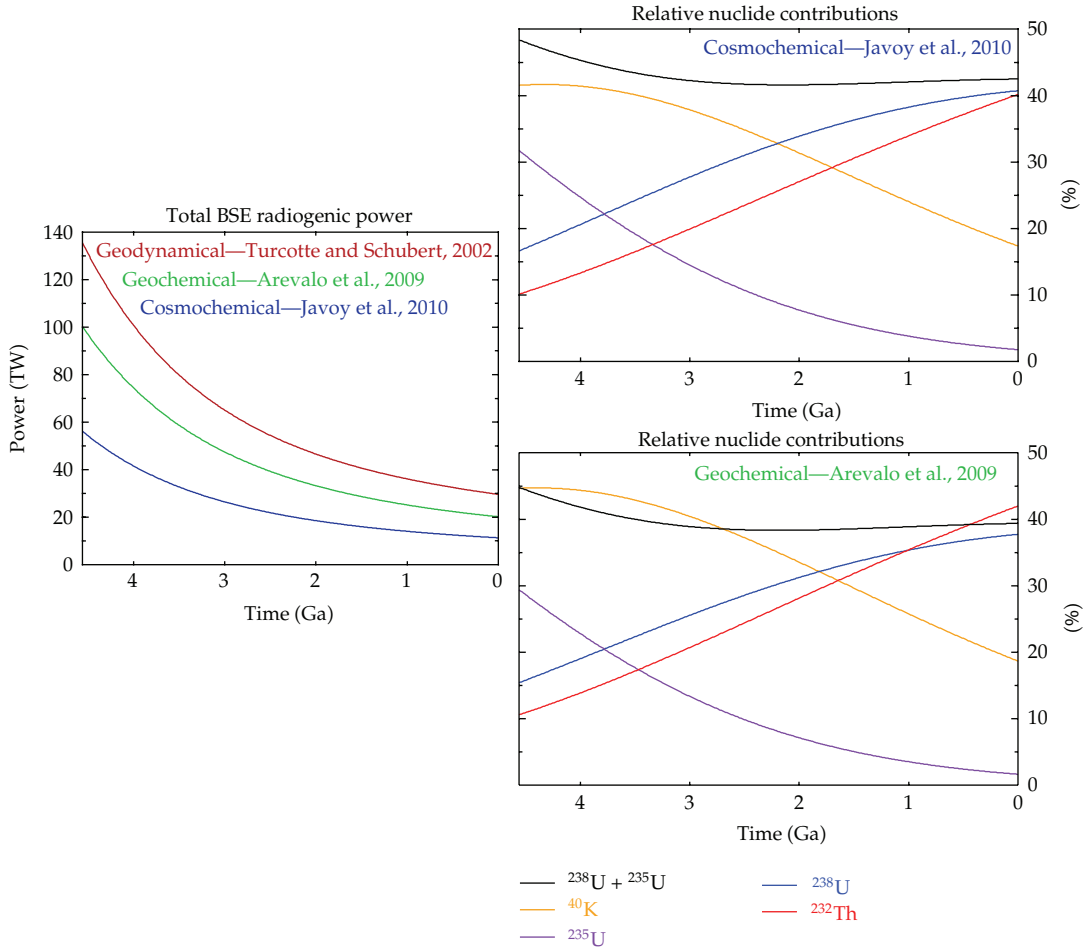


**Figure 2:** (left) Total radiogenic power over Earth's history as predicted by cosmochemical, geochemical, and geodynamical BSE estimates. (right) Relative contributions of each radionuclide for cosmochemical (top) and geochemical (bottom) estimates.

Further uncertainty pertains to the spatial distribution of HPEs in the mantle and the architecture of the mantle in general. Analyses of MORBs reveal the composition of their source region in the shallow mantle. When compared to BSE abundances, one concludes that neither the geochemical nor geodynamical mantle can consist entirely of MORB source material. Mass balances require the existence of a mantle volume enriched in HPEs, and some other elements as well. This has been a long-standing issue in geophysics [81]. Early models argued for mantle layering at ~660 km depth, which separated the shallow depleted mantle (DM) from the deep layer of primordial composition with supposedly no mixing between these two reservoirs. This picture was overturned when seismologists began to image slabs subducting into the deep mantle [82, 83]. Current ideas still embrace the possibility of a mantle reservoir enriched in incompatible elements, but place it much deeper. One suggestion employs the anomalous, possibly partially molten "ultra-low velocity zones" (ULVZ) in the "D" layer of the deepest mantle [84, 85]. Another consideration are the two "large low shear-wave velocity provinces" (LLSVPs) in deep mantle below the Pacific and below Africa

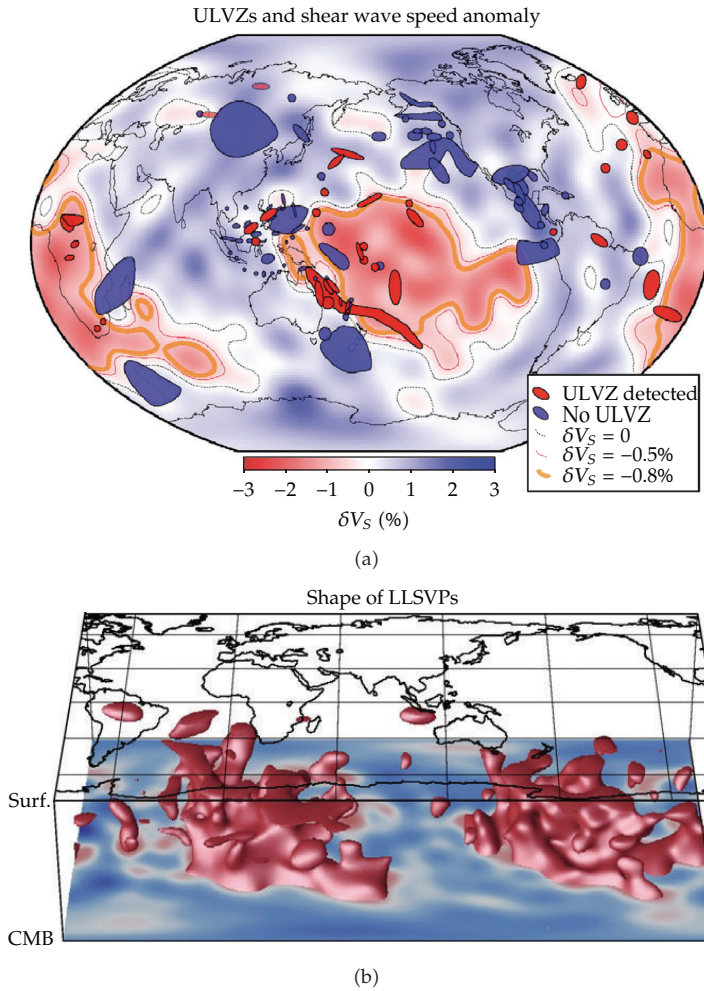


**Figure 3:** (a) Locations where ULVZ was detected superimposed on color map of shear wave speed anomaly ($\delta V_S$) at CMB. (b) Isocontour of $\delta V_S$ showing the 3D structure of LLSVPs below Africa and the Pacific. Based on seismic model S20RTS [93, 94]. Reprinted from [86, 95] with permission from Elsevier.

[85, 86]. In addition to lower-than-average shear wave seismic speeds, the LLSVPs seem to be bounded by sharp velocity gradients [87] and show anticorrelation between shear and bulk sound speeds [88], observations which support a compositional component to the seismic speed anomaly. Figure 3 shows the location of seismically detected ULVZ as well as the shape of the LLSVPs. It was proposed that such a deep-mantle geochemical reservoir may have formed very early in Earth's history [89–92].

The cosmochemical BSE estimate, unlike the geochemical and geodynamical models, is consistent with a uniform composition of the whole mantle and may even show HPE depletion in the lower mantle [64]. The bulk composition of the silicate Earth remains a hotly debated issue and an area of current active research [96–102]. Accurate new information on mantle composition provided by geoneutrino studies is needed. Figure 4 shows a breakdown of the present-day energy budget, which uses the geochemical BSE abundances and includes uncertainties. The mantle cooling rate required to balance the budget was calculated from the

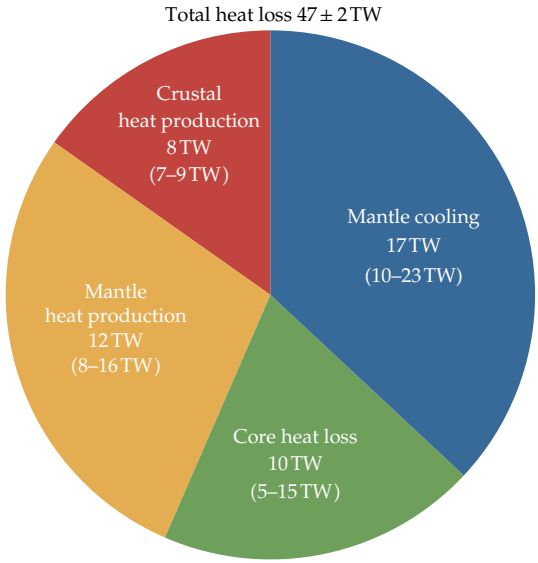


**Figure 4:** Present-day thermal budget of the Earth, which assumes a geochemical BSE composition (~20 TW of radiogenic power). Adapted from [40, 43]. See also [104].

remaining terms in the energy balance. The calculated cooling rate, equivalent of $17 \pm 7$ TW, is higher than a long-term cooling rate estimated by petrological studies of MORB-like rocks, ~50 K Gy$^{-1}$ or ~7 TW [103]. This discrepancy would become even more pronounced with a cosmochemical model for the BSE.

In addition to the aforementioned conventional models, some unorthodox propositions regarding the Earth's composition have been put forward. Even though geochemical arguments strongly disfavor HPEs in the Earth's core, these are discussed in detail in [57], some studies argue for the presence of K [105–107] and even U and Th [108] In the 1970s it was discovered at the uranium mine at Oklo in Gabon, Africa that a natural fast breeder nuclear georeactor had operated there at around 1.8 Ga [109]. Some argue for a present-day operation of such a georeactor at depth in the core-mantle boundary region [110] or in the center of the Earth [111]. This would affect the terrestrial antineutrino production as well and Earth's radioactivity budget, and can be, in essence, resolved by geoneutrino studies.

In summary, these are the fundamental questions geophysics asks, which can be addressed by terrestrial antineutrino detection:

(i) How much U, Th, and K are there in the Earth? (Or equivalently, what is the planetary U abundance and Th/U and K/U ratios?)

(ii) Is the mantle chemically uniform, layered, or more complicated? (Presence of a mantle reservoir enriched in HPEs?)

(iii) Is there radioactivity in the core?

(iv) Is there an operating nuclear georeactor?

As we discuss in detail later, while some of these questions can, in principle, be—and have been—addressed using existing detection methods by accurate measurement at specific locations, answering others will require development of new detection mechanisms. In particular, this applies to antineutrinos from potassium decay, which are not detectable

with the currently used inverse $\beta$-decay mechanism. Current analyses of U + Th geoneutrino flux also have insufficient sensitivity to Th/U ratio.

## 3. Geoneutrino Production

Electron antineutrinos ($\overline{\nu}_e$) are generated upon transmutation of neutron-rich nuclei by $\beta$-decay, accompanied by emission of an electron ($e^-$) and release of decay energy ($Q_\beta$),

$$ {}^{A}_{Z}X \longrightarrow {}^{A}_{Z+1}X' + e^- + \overline{\nu}_e + Q_\beta, \tag{3.1} $$

where $A$ is the mass (nucleon) number, and $Z$ is the atomic (proton) number. Part of the decay energy $Q_\beta = Q_\nu + Q_h$ is carried away by antineutrinos ($Q_\nu$), the remainder is available for heating ($Q_h$). Geologically important isotopes of U, Th, and K that heat the Earth's interior decay into stable nuclei according to [36, 37, 39]:

$$ \begin{aligned} {}^{238}_{92}\mathrm{U} &\longrightarrow {}^{206}_{82}\mathrm{Pb} + 8\alpha + 6e^- + 6\overline{\nu}_e + 51.698\,\mathrm{MeV}, \\ {}^{235}_{92}\mathrm{U} &\longrightarrow {}^{207}_{82}\mathrm{Pb} + 7\alpha + 4e^- + 4\overline{\nu}_e + 46.402\,\mathrm{MeV}, \\ {}^{232}_{90}\mathrm{Th} &\longrightarrow {}^{208}_{82}\mathrm{Pb} + 6\alpha + 4e^- + 4\overline{\nu}_e + 42.652\,\mathrm{MeV}, \\ {}^{40}_{19}\mathrm{K} &\xrightarrow{89.3\%} {}^{40}_{20}\mathrm{Ca} + e^- + \overline{\nu}_e + 1.311\,\mathrm{MeV}, \\ {}^{40}_{19}\mathrm{K} + e^- &\xrightarrow{10.7\%} {}^{40}_{18}\mathrm{Ar} + \nu_e + 1.505\,\mathrm{MeV}. \end{aligned} \tag{3.2} $$

Decay of $^{40}$K branches into $\beta$-decay and electron capture. The complete decay networks can be found in Fiorentini et al. [37]. The decay networks of $^{238}$U and $^{232}$Th contain nine and five $\beta$-decaying nuclei, respectively. Decay energies are taken from Dye [39], who used inputs from the standard table of atomic masses [112]. The antineutrino energy spectra are needed in order to assess detection possibilities and to determine available energy for heating. Spectrum for each decay chain comes from all $\beta$-transitions within that chain, and depends on branching ratios, decay constants, fractional intensities, and energy spectra of the individual transitions [37, 39]. The individual energy spectra are calculated using the Fermi theory of $\beta$-decay. The calculations are laid out in Fiorentini et al. [37], and the inputs are available in the table of isotopes [113] (data available online at http://isotopes.lbl.gov/education/isotopes.htm). Fiorentini et al. [114] propose that theoretically calculated decay spectra should be compared to directly measured spectra.

The antineutrino energy spectra for the three decay chains and $^{40}$K $\beta$-decay in (3.2) are shown in Figure 5(a). For each decay, the average energy of the spectrum multiplied by the number of antineutrinos $n_\nu$ emitted per chain yields the energy carried away by antineutrinos. The remainder $Q_h$ of the decay energy heats the Earth per decay of a parent

**Table 3:** Atomic parameters ($X$, $\mu$, $\lambda$, $\tau_{1/2}$, and $n_\nu$), total and heating energies per decay ($Q$, $Q_h$), specific heating rates ($h$), and antineutrino luminosities ($l$) per unit mass of radionuclide. Adapted from Dye [39].

| | | $^{238}$U | $^{235}$U | $^{232}$Th | $^{40}$K |
|---|---|---|---|---|---|
| Natural isotopic fraction | $X$ | 0.9927 | 0.007204 | 1.000000 | 0.000117 |
| Atomic mass | $\mu$ (g mol$^{-1}$) | 238.051 | 235.044 | 232.038 | 39.9640 |
| Decay constant | $\lambda$ ($10^{-18}$ s$^{-1}$) | 4.916 | 31.210 | 1.563 | 17.200 |
| Half life | $\tau_{1/2}$ (Gy) | 4.468 | 0.7038 | 14.05 | 1.277 |
| Decay energy | $Q$ (pJ) | 8.282 | 7.434 | 6.833 | 0.213 |
| Energy for heating | $Q_h$ (pJ) | 7.648 | 7.108 | 6.475 | 0.110 |
| Specific heat generation | $h$ ($\mu$W kg$^{-1}$) | 95.13 | 568.47 | 26.28 | 28.47$^{\ddagger}$ |
| $\overline{\nu}_e$'s per chain | $n_\nu$ | 6 | 4 | 4 | 0.893$^{\dagger}$ |
| Specific $\overline{\nu}_e$ luminosity | $l$ (kg$^{-1}$ $\mu$s$^{-1}$) | 74.6 | 319.9 | 16.2 | 231.2 |

$^{\dagger}$Noninteger $\overline{\nu}_e$'s per chain value for $^{40}$K reflects branching into $\beta$ decay and electron capture. $^{\ddagger}$Heat generation from $^{40}$K includes energy heat released in electron capture.

**Table 4:** Specific heat generation $h_{el}$ and antineutrino luminosity $l_{el}$, per unit mass of element. From Dye.

| | U | Th | K |
|---|---|---|---|
| $h_{\text{el}}$ ($\mu$W kg$^{-1}$) | 98.5 | 26.3 | 0.00333 |
| $l_{\text{el}}$ (kg$^{-1}$ $\mu$s$^{-1}$) | 76.4 | 16.2 | 0.0271 |

nuclide. Specific heating rates $h$ and specific antineutrino luminosities $l$, per unit mass of each parent nuclide, can be calculated from

$$h = \frac{\lambda N_A Q_h}{\mu}, \tag{3.3}$$

$$l = \frac{\lambda N_A n_\nu}{\mu}, \tag{3.4}$$

where $\lambda$ is decay constant, $\mu$ is molar mass, and $N_A$ is Avogadro's number. Heating rates $h_{el}$ and luminosities $l_{el}$ per unit mass of element are sums of isotopic values weighted by isotopic abundances $X$,

$$l_{el} = \sum_{\text{nuclides}} Xl, \tag{3.5}$$

and similarly for $h_{el}$. The atomic parameters, decay energies per decay, and specific heating rates and antineutrino luminosities per unit mass of radionuclide, as reported by [39], are listed in Table 3. The heating rates and luminosities per unit mass of element are shown in Table 4. When the total decay powers and heating powers (per unit mass of rock) are evaluated for various BSE compositions (Table 2), it follows that ~80% of decay energy heats the planet's interior while the remaining ~ 20% is carried away by geoneutrinos [39]. This result is roughly independent of the choice of BSE model since the Th/U and K/U ratios are similar between all BSE estimates.

## 4. Geoneutrino Oscillation

Neutrino oscillations (albeit $\nu$-$\bar{\nu}$ oscillation) were first hypothesized by Pontecorvo in 1957 [115] and have now been observed as neutrino flavor oscillation for solar, atmospheric, reactor, and accelerator-produced neutrinos. (Neutral current—neutrino in and neutrino out, no charged lepton—interactions are also possible for all neutrino flavors, but in practice here, are negligible in rate for a given visible energy.) Of the three flavors, only the terrestrial electron antineutrino is detectable by the neutron inverse $\beta$-decay mechanism, which reduces the observable geoneutrino signal. Most recently the evidence [116] for a nonzero value of the last mixing angle of three-flavor oscillation was confirmed [117, 118]. The three-flavor survival probability of electron antineutrino of energy $E_\nu$ after flying a distance $L$ is [39]

$$P_{ee}^{3\nu}(E_\nu, L) = 1 - \Big\{\cos^4\theta_{13}\sin^2 2\theta_{12}\sin^2\Delta_{21} + \sin^2 2\theta_{13}\Big[\cos^2 2\theta_{12}\sin^2\Delta_{31} + \sin^2 2\theta_{12}\sin^2\Delta_{32}\Big]\Big\}, \tag{4.1}$$

where $\theta_{12}$ and $\theta_{13}$ are mixing angles,

$$\Delta_{ij}(E_\nu, L) = \frac{1.27\left|\delta m_{ji}^2\left[\mathrm{eV}^2\right]\right|L[\mathrm{m}]}{E_\nu[\mathrm{MeV}]}, \tag{4.2}$$

and $\delta m_{ji}^2 = m_j^2 - m_i^2$ is the neutrino mass-squared difference (by definition $\delta_{31}^2 = \delta_{32}^2 + \delta_{21}^2$). Given the small value of $\delta_{21}^2$ relative to $\delta_{31}^2 \approx \delta_{32}^2$ [119] (~3%), the survival probability (4.1) can be approximated by

$$P_{ee}(E_\nu, L) = 1 - \left[\cos^4\theta_{13}\sin^2 2\theta_{12}\sin^2\Delta_{21} + \frac{1}{2}\sin^2 2\theta_{13}\right]. \tag{4.3}$$

The oscillation length for antineutrinos with energies within the detectable range (1.8–3.3 MeV) is 60–110 km. Given the Earth's radius of ≈6400 km, the average survival probability,

$$\langle P_{ee}\rangle = 1 - \frac{1}{2}\left[\cos^4\theta_{13}\sin^2 2\theta_{12} + \sin^2 2\theta_{13}\right] = 0.544^{+0.017}_{-0.013}, \tag{4.4}$$

can be used to oscillate the terrestrial antineutrino flux, which only introduces minimal error. According to analysis by Dye [39], the use of average survival probability underestimates the geoneutrino flux at the detector location. This effect comes from radionuclides distributed within the first oscillation length around the detector and is more pronounced at higher antineutrino energies. In oceanic regions with a thin and less enriched oceanic crust, the underestimation does not exceed 1%. It can reach few percent over continents. There are also interesting effects due to "matter effects" and the order of the neutrino masses, but they are negligible for our concerns herein.

## 5. Geoneutrino Flux

The fully oscillated geoneutrino flux spectrum from each radionuclide at observation location $\vec{r}$ is calculated from [36]

$$\frac{\mathrm{d}\phi(E_\nu,\vec{r})}{\mathrm{d}E_\nu} = \frac{Xl}{n_\nu}\frac{\mathrm{d}n(E_\nu)}{\mathrm{d}E_\nu}\int_\Omega \mathrm{d}^3\vec{r}^{\,\prime}\,\frac{A\left(\vec{r}^{\,\prime}\right)\rho\left(\vec{r}^{\,\prime}\right)P_{ee}\left(E_\nu,\left|\vec{r}-\vec{r}^{\,\prime}\right|\right)}{4\pi\left|\vec{r}-\vec{r}^{\,\prime}\right|^2}, \tag{5.1}$$

where $\mathrm{d}n(E_\nu)/\mathrm{d}E_\nu$ is the intensity energy spectrum, and $\Omega$ is the volumetric domain with rock of density $\rho$ that contains HPEs with elemental abundance $A$ (mass of element per unit mass of rock). For an emission domain of uniform composition and using the average survival probability, (5.1) simplifies to yield the flux from a given radionuclide:

$$\phi(\vec{r}) = XlA\langle P_{ee}\rangle\int_\Omega \mathrm{d}^3\vec{r}^{\,\prime}\,\frac{\rho\left(\vec{r}^{\,\prime}\right)}{4\pi\left|\vec{r}-\vec{r}^{\,\prime}\right|^2}. \tag{5.2}$$

The integral in (5.2) has been traditionally defined as the geological response factor $G$ [15],

$$G \equiv \int_\Omega \mathrm{d}^3\vec{r}^{\,\prime}\,\frac{\rho\left(\vec{r}^{\,\prime}\right)}{4\pi\left|\vec{r}-\vec{r}^{\,\prime}\right|^2}. \tag{5.3}$$

For a uniform density spherical shell geoneutrino emission domain bounded by radii $r_1$ and $r_2$, both are smaller than the observation point radius $a$ (~Earth's radius), the integral can be evaluated exactly [15, 37] (note that this is a different situation than that in calculating the force of gravity from a shell, as this is a scalar addition not vector, and there is no cancellation of opposing transverse components),

$$\begin{aligned} G_{\substack{\text{unif.}\\ \text{shell}}} &= \frac{\rho}{4\pi}\int_{r_1}^{r_2}\mathrm{d}r'\int_0^{\pi}\mathrm{d}\vartheta'\int_0^{2\pi}\mathrm{d}\varphi'\,\frac{r'^2\sin\vartheta'}{a^2+r'^2-2ar'\cos\vartheta'} \\ &= \frac{\rho a}{4}\left[2\frac{r_2-r_1}{a}-\left(1-\frac{r_2^2}{a^2}\right)\ln\left(\frac{a+r_2}{a-r_2}\right)+\left(1-\frac{r_1^2}{a^2}\right)\ln\left(\frac{a+r_1}{a-r_1}\right)\right]. \end{aligned} \tag{5.4}$$

## 6. Geoneutrino Detection

The same detection mechanism that Reines and Cowan [120, 121] used in their pioneering experiment is employed in present-day geoneutrino-counting detectors. It uses the neutron inverse $\beta$-decay process, where an electron antineutrino scatters on a free proton to produce a neutron and a positron,

$$\overline{\nu}_e + p \rightarrow e^+ + n. \tag{6.1}$$

A subsequent prompt annihilation of the positron with an electron and delayed capture of neutron on a proton provide light flashes in a scintillating liquid, coincident in time

and in space, which offers a powerful method for identification of antineutrino events and elimination of single-flash background (Figure 6). Reaction (6.1) works for antineutrinos with energies $E_\nu$ above the kinematic threshold, the difference between rest mass energies of neutron plus positron and proton, $\Delta + m_e = 1.804\,\text{MeV}$, where $\Delta = M_n - M_p$.

The positron carries most of the energy, its starting kinetic energy being $T_e \approx E_\nu - 1.8\,\text{MeV}$. The prompt signal of the positron annihilation with an electron in the medium,

$$e^+ + e^- \rightarrow \gamma + \gamma, \tag{6.2}$$

comes within few nanoseconds of the antineutrino interaction in currently used organic scintillating liquids. The energy of the light flash $E_{\text{vis1}}$ scales with the incident antineutrino energy, $E_{\text{vis1}} \approx T_e + 2m_e = E_\nu - 0.8\,\text{MeV}$. The neutron receives most of the antineutrino momentum. It slows down and in 20–200 $\mu$s combines with a proton in the medium to form a deuteron,

$$n + p \rightarrow d + \gamma. \tag{6.3}$$

The release of deuteron binding energy of 2.2 MeV causes a second light flash in the scintillating medium.

Above the threshold energy ($\approx$1.8 MeV) of reaction (6.1), the cross-section scales with the square of the positron energy $E_e = E_\nu - \Delta$ [123]. Written in terms of antineutrino energy,

$$\sigma(E_\nu) = 9.52(E_\nu - \Delta)^2 \sqrt{1 - \frac{m_e^2}{(E_\nu - \Delta)^2}} \times 10^{-44}\,\text{cm}^2, \tag{6.4}$$

where $E_\nu$, $\Delta$, and $m_e$ are in MeV. The cross-section is plotted in Figure 5(b). For each decay chain, the product of antineutrino intensity energy spectrum with the cross-section yields the interaction energy spectrum (Figure 5(c)). Out of the nine $\beta$-decaying nuclei in the $^{238}$U decay network, only three nuclides ($^{234}$Pa, $^{214}$Bi, and $^{210}$Tl) emit antineutrinos with energy exceeding the detection threshold 1.8 MeV. One transition of $^{234}$Pa together with two transitions of $^{214}$Bi accounts for 99.8% of signal from $^{238}$U decay chain [114]. In $^{232}$Th decay chain, only two nuclides ($^{228}$Ac, $^{212}$Bi) emit detectable antineutrinos, and 99.8% of the signal comes from one transition of $^{212}$Bi and the first of two transitions of $^{228}$Ac [114]. Antineutrinos from $^{40}$K of maximum energy 1.311 MeV, as well as $^{235}$U antineutrinos, are below the threshold of inverse beta decay. This is inconvenient for geophysics as information on terrestrial K is desirable.

The cross-section of inverse $\beta$-decay reaction (6.4) is extremely small. In their 1950's experiment, Cowan and Reines used a cubic meter-sized detector placed some 10 m from Savannah River power. With the high reactor antineutrino flux they achieved an event rate of up to ~3 events per hour [10]. A typical detectable geoneutrino flux from the entire Earth is of the order of $10^6\,\text{cm}^{-2}\text{s}^{-1}$. It requires an order of $10^{32}$ free protons to reach reasonable interaction rates (tens of events per year). This translates into a required detector mass of $\gtrsim$1 kiloton.

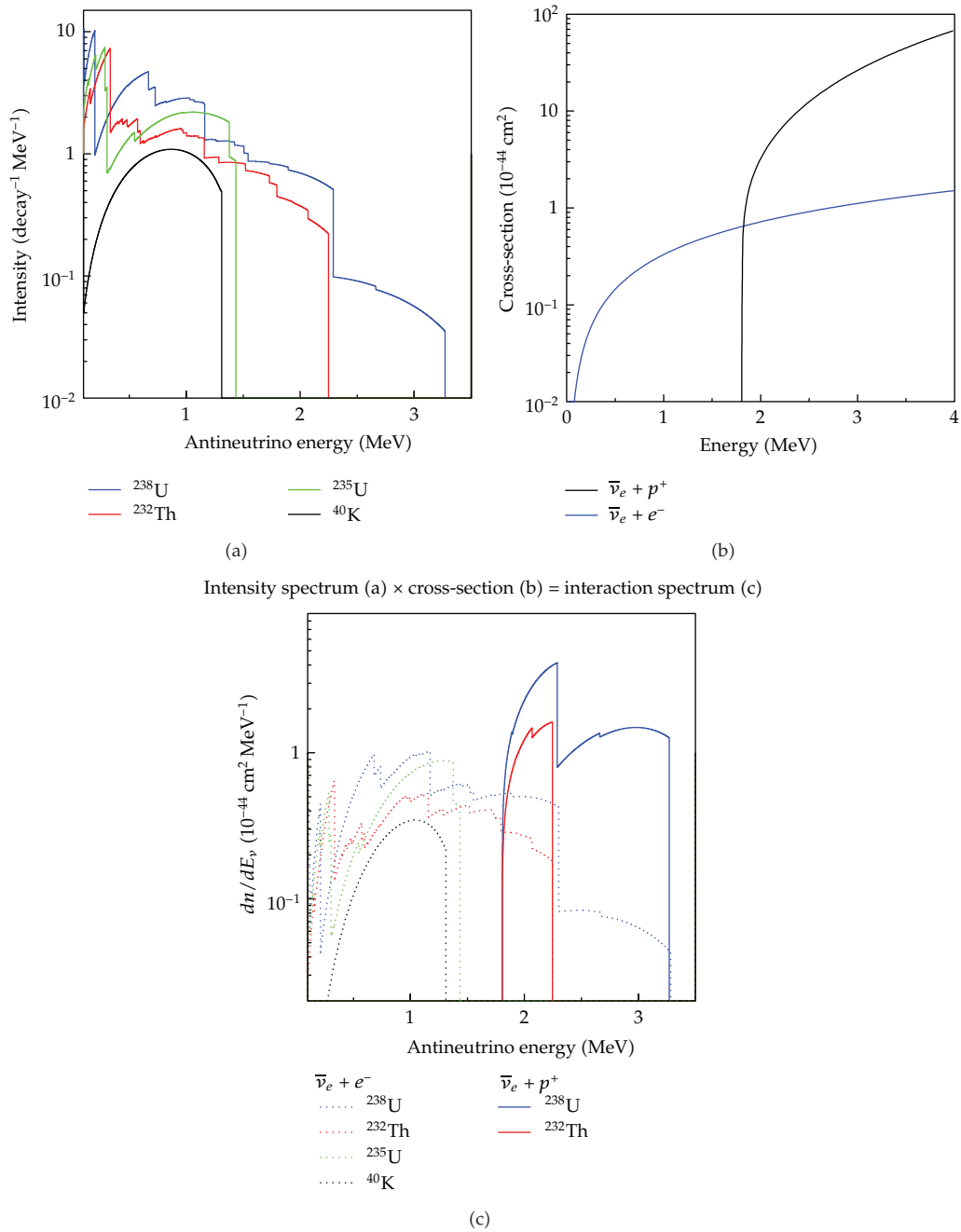


**Figure 5:** (a) Antineutrino intensity energy spectra. The area below each curve equals the number of antineutrinos $n_\nu$ emitted per decay. (b) Total cross-sections for scattering of antineutrinos on protons and electrons. (c) Antineutrino interaction energy spectra per decay of parent nuclide. Solid lines in (b) and (c) show antineutrino scattering on protons; dashed lines show scattering on electrons. Adapted from [39], reproduced/modified by permission of American Geophysical Union.

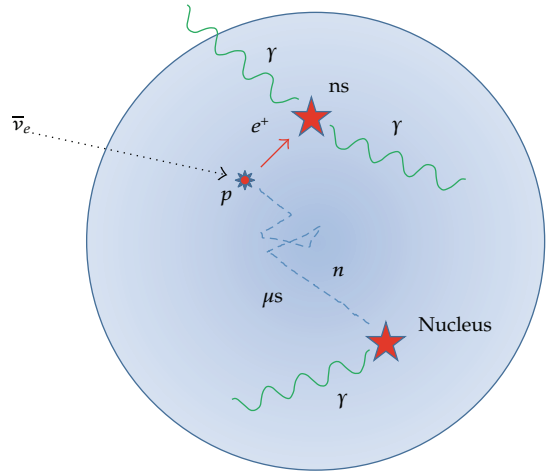


**Figure 6:** Schematic of antineutrino detection by scattering on protons. Prompt signal comes from positron annihilation, delayed signal occurs when neutron captures a proton.

Similarly to (5.1) for antineutrino flux spectrum, the event spectrum of detection at efficiency $\varepsilon$ is

$$\frac{\mathrm{d}N(E_\nu,\vec{r})}{\mathrm{d}E_\nu} = \frac{\varepsilon X l}{n_\nu}\frac{\mathrm{d}n(E_\nu)}{\mathrm{d}E_\nu}\sigma(E_\nu)\int_\Omega \mathrm{d}^3\vec{r}^{\,\prime}\,\frac{A\left(\vec{r}^{\,\prime}\right)\rho\left(\vec{r}^{\,\prime}\right)P_{ee}\left(E_\nu,\left|\vec{r}-\vec{r}^{\,\prime}\right|\right)}{4\pi|\vec{r}-\vec{r}^{\,\prime}|^2}, \tag{6.5}$$

where $\sigma(E_\nu)\mathrm{d}n(E_\nu)/\mathrm{d}E_\nu$ is the interaction spectrum. For emission from a uniform composition domain and with the average survival probability, (6.5) simplifies to

$$N(\vec{r}) = \frac{\varepsilon X l A\langle P_{ee}\rangle G}{C}, \tag{6.6}$$

where a conversion factor $C$ was introduced such that

$$\frac{1}{C} = \frac{1}{n_\nu}\int \mathrm{d}E_\nu \frac{\mathrm{d}n(E_\nu)}{\mathrm{d}E_\nu}\sigma(E_\nu). \tag{6.7}$$

It relates the antineutrino event rate $N$ (number of events detected per unit time) to the antineutrino flux $\phi$ (number or $\overline{\nu}_e$ per unit area and unit time) at the detector. Comparing (5.2) and (6.6), we arrive at

$$N = \frac{\varepsilon\phi}{C}. \tag{6.8}$$

It is convenient to introduce the signal rate $R$ (number of interactions per unit time) counted in "terrestrial neutrino unit" (TNU), defined as one interaction over a year-long fully efficient exposure of $10^{32}$ free protons [124]. Unlike the event rate $N$ which depends on detector size

and efficiency of detection $\varepsilon$, the signal rate $R$ only depends on the detection mechanism. It follows that

$$R = \frac{\phi}{C} = \frac{XlA\langle P_{ee}\rangle G}{C}. \tag{6.9}$$

The signal-rate-to-flux conversion factors are [36, 37, 39]

$$\begin{aligned} C_{\mathrm{U}} &= 7.6 \times 10^{4}\ \mathrm{cm^{-2}\,s^{-1}\,TNU^{-1}}, \\ C_{\mathrm{Th}} &= 2.5 \times 10^{5}\ \mathrm{cm^{-2}\,s^{-1}\,TNU^{-1}}. \end{aligned} \tag{6.10}$$

Radiogenic heat generated in a uniform composition domain of mass $M$ is

$$H = XhAM. \tag{6.11}$$

Equations (6.9) and (6.11) provide a proportionality relation between signal rate $R$ or flux $\phi$ and heat production $H$,

$$\begin{aligned} R &= \frac{\langle P_{ee}\rangle}{C}\frac{G}{M}\frac{l}{h}H, \\ \phi &= \langle P_{ee}\rangle \frac{G}{M}\frac{l}{h}H, \end{aligned} \tag{6.12}$$

coming from each radionuclide. For a given Th to U abundance ratio, $\kappa \equiv A_{\mathrm{Th}}/A_{\mathrm{U}}$, we get the following heating, flux, and signal rate ratios:

$$\begin{aligned} \frac{H_{\mathrm{Th}}}{H_{\mathrm{U}}} &= \frac{X_{\mathrm{Th}}h_{\mathrm{Th}}}{X_{\mathrm{U}}h_{\mathrm{U}}}\kappa = 0.278\ \kappa, \\ \frac{\phi_{\mathrm{Th}}}{\phi_{\mathrm{U}}} &= \frac{X_{\mathrm{Th}}l_{\mathrm{Th}}}{X_{\mathrm{U}}l_{\mathrm{U}}}\kappa = 0.219\ \kappa, \\ \frac{R_{\mathrm{Th}}}{R_{\mathrm{U}}} &= \frac{C_{\mathrm{U}}}{C_{\mathrm{Th}}}\frac{\phi_{\mathrm{Th}}}{\phi_{\mathrm{U}}}\kappa = 0.066\ \kappa. \end{aligned} \tag{6.13}$$

For a whole Earth Th/U ratio of 4.0 [60], these relations imply that while radiogenic heating and the geoneutrino flux are contributed roughly equally by $^{232}$Th and $^{238}$U (53% and 47%, resp., come from from Th and U), only 21% of detected signal is comes from Th. Table 5 lists the masses $M$ and geological response factors $G$ for Earth reservoirs.

Background signal adds to the geologically interesting signal in the geoneutrino energy range. Background signal consists of nuclear reactor antineutrinos, fast neutrons generated by cosmic ray muon interactions, long-lived neutron-rich radionuclides ($^{8}$He and $^{9}$Li), $^{13}\mathrm{C}(\alpha, n)^{16}\mathrm{O}$ reaction, and accidental $\gamma$-ray background. It is important to realize that inverse $\beta$-decay provides strong rejection to single-hit backgrounds such as those from solar neutrinos. Requiring two hits close in spaces and time, with the second (delayed hit being of

**Table 5:** Masses of Earth reservoirs $M$ and geological response factors $G$ (5.3) based on PREM [125], where each reservoir is a spherical shell of uniform thickness. More precise crustal mass calculated using a seismically determined crustal structure (model CRUST2.0 [126]) is also included.

| | $M$ ($10^{24}$ kg) | $G$ ($10^{10}$ kg m$^{-2}$) |
|---|---|---|
| Crust | 0.0312 (C2: 0.0277) | 0.0218 |
| Mantle | 4.00 | 1.18 |
| Outer core | 1.84 | 0.386 |
| Inner core | 0.0984 | 0.0194 |
| Earth | 5.97 | 1.60 |

**Table 6:** Geographical location, size, and depth of geoneutrino detectors. Size in number of free protons, depth in meter water equivalent. Adapted from [38].

| Detector | Location | Lat. °N | Lon. °E | Free $p$ $10^{32}$ | Depth m.w.e. |
|---|---|---|---|---|---|
| *Operating or under construction* | | | | | |
| KamLAND | Kamioka, Japan | 36.43 | 137.31 | 0.6 | 2700 |
| Borexino | LNGS, Gran Sasso, Italy | 42.45 | 13.57 | 0.1 | 3700 |
| SNO+ | SNOLAB, Sudbury, Ontario, Canada | 46.47 | −81.20 | 0.6 | 6000 |
| *Proposed* | | | | | |
| LENA | CUPP, Pyhäsalmi, Finland | 63.66 | 26.05 | 36.7 | 4000 |
| Homestake | DUSEL, Lead, South Dakota, USA | 44.35 | −103.75 | 0.5 | 4500 |
| Baksan | BNO, Caucasus, Russia | 43.29 | 42.70 | 4.0 | 4800 |
| Daya Bay II | Daya Bay, China | | | 8–42 | |
| Hanohano | Pacific | 19.72 | −156.32 | 7.3 | 4500 |

known energy, is a very powerful tool for rejecting most backgrounds. Complete discussion and estimates of the background are presented in Dye [39].

Another possible mechanism for geoneutrino detection involves antineutrino scattering on electrons [127], which would broaden the energy range of detectable geoneutrinos below the 1.8 MeV energy threshold of inverse $\beta$-decay including signal from $^{40}$K decay. The interaction cross-sections and antineutrino energy spectra are shown in Figure 5. While the lack of a coincidence tag makes the detection challenging, the recoiling electrons offer the possibility to determine the direction of the incoming antineutrino [39]. The electron events can be recorded in a device such as the miniTimeCube [128] near a reactor as a demonstration. Further development is needed before this method can be employed for geoneutrino detection.

## 7. Detectors

Instruments capable of geoneutrino detection contain a large volume of liquid scintillator (LS), monitored by inward facing photomultiplier tubes (PMTs), and are operated underground in order to reduce the cosmic-ray-induced atmospheric muon flux. They are used to investigate neutrino oscillations, nucleon decay, issues in astrophysics and geophysics, and to monitor nuclear reactors. Table 6 lists selected parameters of operating and proposed geoneutrino detectors.

KamLAND (Kamioka liquid-scintillator antineutrino detector, website at http://www.awa.tohoku.ac.jp/KamLAND/), is a 1 kiloton LS detector located 1 km underground beneath Mt. Ikenoyama summit in the old Kamioka zinc mine, Japan. The LS is composed of 80% of dodecane (diluter), 20% of pseudocumene (energy transferor), and 1.36 g liter$^{-1}$ of diphenyloxazole (PPO, scintillating molecule). The fiducial volume is monitored by ~1900 PMTs, which cover 34% of the surface area. Number of free protons is $\sim 6 \times 10^{23}$, and detection efficiency is 80.7% and 75.1% for signals from U and Th, respectively [19, 31].

Borexino (website at http://borex.lngs.infn.it/) is a 278-ton LS detector at Laboratori Nazionali del Gran Sasso (LNGS) located midway a 10 km long highway tunnel below the Central Apennine Mountains in Italy. The scintillating liquid is pseudocumene doped with 1.5 g liter$^{-1}$ of PPO. Scintillations are monitored by ~2200 PMTs covering 30% of surface area [20, 129].

SNO+ (website at http://snoplus.phy.queensu.ca/) is a follow-up experiment to SNO (Sudbury Neutrino Observatory) at SNOLAB near Sudbury, Ontario, Canada. Located 2 km underground in a nickel mine, it will be refilled with linear alkylbenzene (LAB) LS. It is expected to become operational in 2013.

Several other geoneutrino-detecting experiments have been proposed: LENA (website at http://www.e15.ph.tum.de/research_and_projects/lena/), a 50-kiloton detector at the Center for Underground Particle Physics (CUPP) located at the Pyhäsalmi mine near Pyhäjärvi, Finland [130]; Homestake at the Deep Underground Science and Engineering Laboratory (DUSEL) in Lead, South Dakota, USA [131]; Baksan at the Baksan Neutrino Observatory (BNO) in Russia [132]; Hanohano (online information at http://www.phys.hawaii.edu/~jgl/hanohano.html), a 10–50 kiloton ocean-faring transportable detector based in Hawaii [133, 134]; a 10–50 kiloton detector of the Daya Bay II experiment [135].

## 8. Earth's Reference Model and Flux Prediction

The development of reference models for terrestrial antineutrino emission and evaluation of geoneutrino flux predictions is critical for two main reasons. First, these predictions guide the design of geoneutrino detectors. Second, they are necessary for interpretation of the antineutrino data. Since the first attempts in the 1960s [11, 12] and a presentation of systematic approach to geoneutrino predictions by Krauss et al. [15], the emission models have been refined, following advances in both geological sciences and neutrino physics [16–18, 22, 30, 31, 36–39, 69, 124, 136–139].

The geological inputs for calculation of geoneutrino emission are the rock density $\rho(\vec{r})$ and chemical abundances $A(\vec{r})$ of U, Th, and K throughout the Earth's interior. The predicted geoneutrino flux is then calculated from (5.1) and (5.2), respectively, assuming the neutrino physics inputs are known.

### *8.1. Crustal Flux*

The proportionality of antineutrino flux to inverse square source distance means that a significant portion of the signal originates near the observation point. Furthermore, the continental crust is highly enriched in geoneutrino producing HPEs, as was discussed in Section 2. Figure 7, showing cumulative flux within a given distance from a detector,

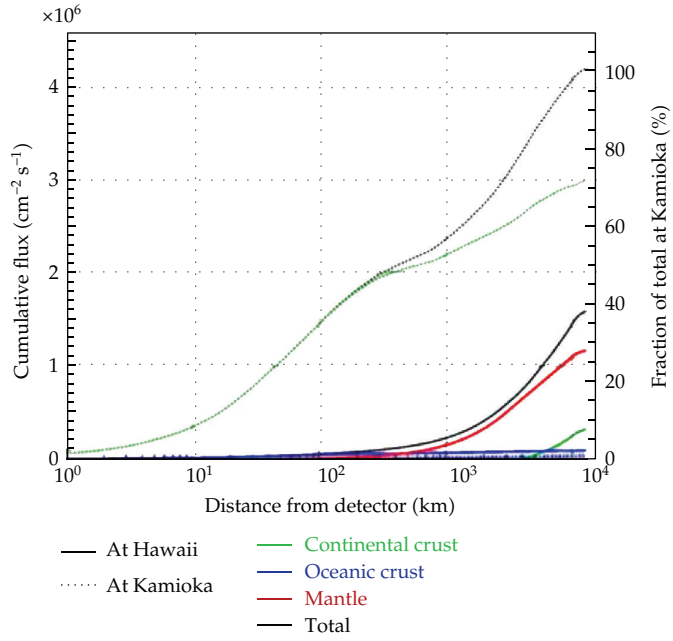


**Figure 7:** Cumulative geoneutrino flux within a given distance from a detector, for observation at Kamioka (continental site) and Hawaii (oceanic site). Reprinted from [36] with permission from Elsevier.

illustrates the point. Both operating geoneutrino detectors, KamLAND and Borexino, as well as SNO+ and all but one of the proposed future experiments are located in continental areas. At Kamioka, for example, ~50% of the signal originates within 500 km distance from the detector, almost exclusively in the continental crust [36]. Any attempts to extract mantle information from geoneutrino data require construction of accurate crustal geological models [31, 36, 37, 39, 124, 136, 137]. This involves constructing a global crustal model and local refinements in the vicinity (few hundred kms) of the detector. Effects of local geology were carefully evaluated for both KamLAND [36, 37, 136] and Borexino [140].

Current global crustal models use CRUST2.0 model of the crustal structure [126], supplemented with estimates of crustal composition coming from petrological studies. CRUST2.0 describes a $2° \times 2°$ tiled, vertically layered crustal geometry; includes rock densities in each of the five rock layers (upper and lower sediments, and upper, middle, and lower crust) in each tile. Chemical abundance estimates are given by Rudnick and Gao [53] for continental crust, White and Klein [141] for oceanic crust, and Plank [142] for oceanic sediments. A new, more detailed reference model for the crust and uppermost mantle is being developed [143].

In Figure 8, we show a global map of predicted crustal geoneutrino signal from [68]. The spatial pattern of the geoneutrino signal correlates with crustal thickness and continental distribution. HPE abundances used in the calculation are listed in Table 7. A- and B-type tiles of CRUST2.0 are considered oceanic, all other tile types are continental. This model outputs $7.8 \pm 0.9$ TW of radiogenic power from continental crust and $0.22 \pm 0.03$ TW from oceanic crust (Table 7).

**Table 7:** HPE abundances used in calculation of the global crustal flux in Figure 8 and calculated abundances for the bulk crust and bulk mantle.

| | U (ppm) | Th (ppm) | K (%) | | |
|---|---|---|---|---|---|
| | | | | Reference | |
| Input for crust calculation | | | | | |
| Upper cont. crust + sed. | $2.7 \pm 21\%$ | $10.5 \pm 10\%$ | $2.32 \pm 10\%$ | [53] | |
| Middle cont. crust | $1.3 \pm 31\%$ | $6.5 \pm 8\%$ | $1.91 \pm 14\%$ | [53] | |
| Lower cont. crust | $0.2 \pm 80\%$ | $1.2 \pm 80\%$ | $0.51 \pm 30\%$ | [53] | |
| Oceanic sediments | $1.73 \pm 9\%$ | $8.10 \pm 7\%$ | $1.83 \pm 7\%$ | [142] | |
| Oceanic crust | $0.07 \pm 30\%$ | $0.21 \pm 30\%$ | $0.072 \pm 30\%$ | [141] | |
| | | | | Th/U | Power TW |
| Bulk crust, calculated | | | | | |
| Bulk continental crust | $1.47 \pm 0.25$ | $6.33 \pm 0.50$ | $1.63 \pm 0.12$ | 4.3 | $7.8 \pm 0.9$ |
| Bulk oceanic crust | $0.15 \pm 0.02$ | $0.58 \pm 0.07$ | $0.16 \pm 0.02$ | 3.9 | $0.22 \pm 0.03$ |
| Bulk crust | $1.17 \pm 0.19$ | $5.02 \pm 0.38$ | $1.30 \pm 0.09$ | 4.3 | $8.1 \pm 0.9$ |
| | U (ppb) | Th (ppb) | K (ppm) | Th/U | Power TW |
| Bulk mantle, calculated | | | | | |
| Cosmochemical mantle | 4.1 | 8.4 | 57 | 2.0 | 3.3 |
| Geochemical mantle | 12 | 46 | 192 | 3.8 | 12 |
| Geodynamical mantle | 23 | 90 | 310 | 3.9 | 22 |

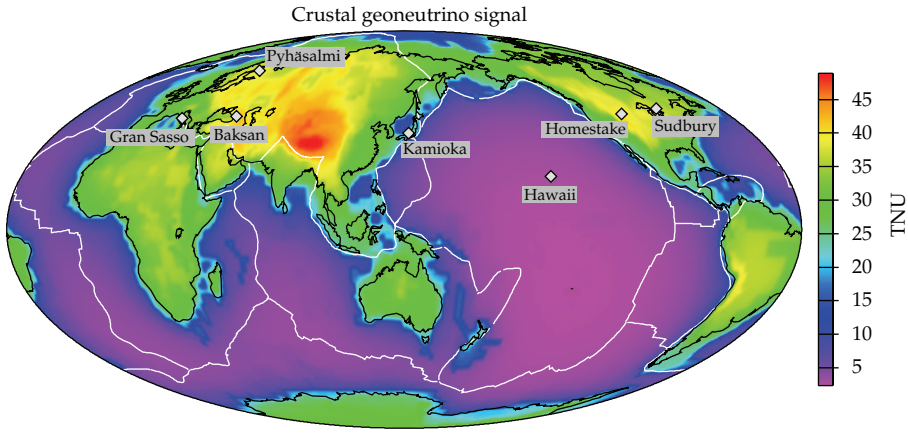


**Figure 8:** Global map of crustal geoneutrino signal (U + Th) in TNU. Prediction is based on CRUST2.0 crustal structure and HPE abundances listed in Table 7. Continental outlines (black), plate boundaries (white), and locations of geoneutrino detectors are plotted. Mollweide equal-area projection was used. See [69].

## *8.2. Mantle Flux*

Density in the Earth increases with depth. In addition to the density increase due to compressibility, pressure induces solid-solid mineral phase transitions which modify the density. For the sake of geoneutrino prediction, lateral density variations caused by temperature anomalies ($\delta\rho \lesssim 1\%$) can be neglected, and only depth-dependent density used, $\rho(\vec{r}) = \rho(r)$. The Preliminary Reference Earth Model (PREM) [125] has been a

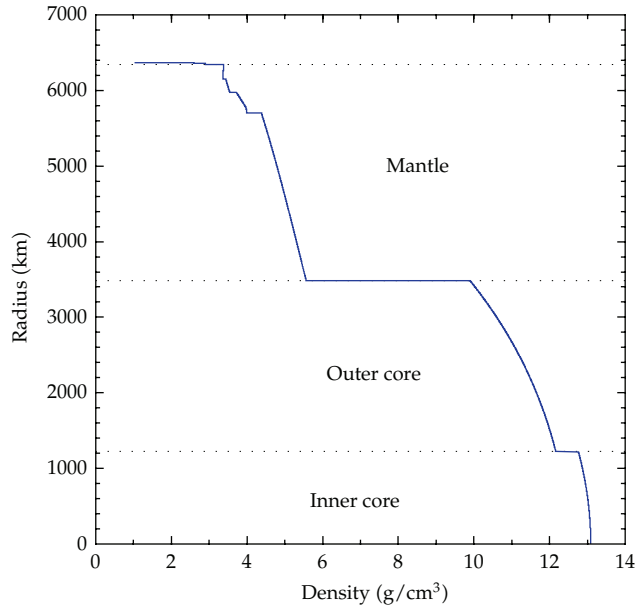


**Figure 9:** Depth dependence of density as given by PREM [125].

**Table 8:** Mantle geoneutrino signal in TNU predicted under the assumption of uniform distribution of U and Th.

| Uniform mantle | $R_U$(TNU) | $R_{Th}$(TNU) | $R_{U+Th}$(TNU) |
|---|---|---|---|
| Cosmochemical mantle | 2.6 | 0.35 | 2.9 |
| Geochemical mantle | 7.5 | 1.9 | 9.4 |
| Geodynamical mantle | 14 | 3.7 | 18 |

standard in geophysics. PREM provides a parameterization of density as a piecewise third-order (at most) polynomial in radius (Figure 9). The density increases from ~3400 kg m$^{-3}$ to ~5600 kg m$^{-3}$ across the mantle.

The average radionuclide abundances in the mantle are calculated from the elemental mass balance as follows:

$$A_{BSE}M_{BSE} = A_{crust}M_{crust} + A_{mantle}M_{mantle}, \tag{8.1}$$

using BSE abundance from Table 2, crustal abundance from Table 7, and the reservoir masses from Table 5. The mantle abundances, based on three different BSE estimates—cosmochemical [64], geochemical [60], and geodynamical [65]—are reported in Table 7. The predicted geoneutrino signal coming from a mantle of uniform composition can be easily evaluated from (6.9). The predictions, listed in Table 8, should be compared to the crustal prediction at continental sites ($\gtrsim$30 TNU, Figure 8) to appreciate the difficulty of extracting information about the mantle from continent-based geoneutrino detection. See [39, 69] for complete treatment including model uncertainties.

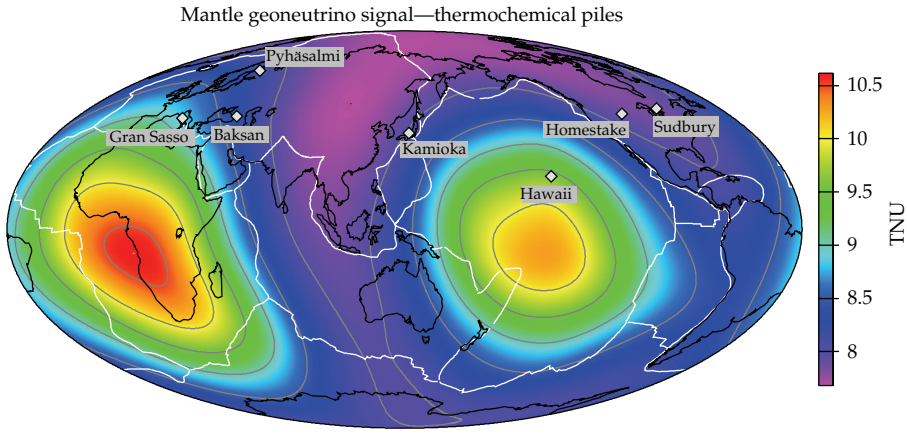


**Figure 10:** Lateral variation of mantle geoneutrino signal predicted for a "thermochemical piles" model. Uses BSE and DM compositional estimates of [60, 68]. See [69].

As we discussed in Section 2, geochemical and geodynamical abundance estimates, combined with compositions inferred for shallow mantle, are not consistent with uniform composition of the whole mantle. The usual fix calls for the existence of a mantle reservoir enriched in incompatible elements. Geophysical observations now disfavor the traditional mantle layering at 660 km depth. An enriched reservoir, however, may exist in the lowermost mantle within few hundred kms of the CMB. The effect of such segregation of HPEs at depth is a decrease in mantle geoneutrino signal [38]. For an enriched layer of uniform thickness atop the CMB, the effect is moderate, with a mantle signal reduction by 25% at most [69]. It has also been suggested that LLSVPs below Africa and Pacific (Figure 3) may be compositionally distinct from the ambient mantle. Consequences of such antipodal deep mantle piles for mantle geoneutrino detection were investigated in [69, 139]. Figure 10 shows the lateral variation of mantle geoneutrino flux predicted for a "thermochemical piles" model, where the piles are enriched in HPEs. The enrichment follows from the compositional estimates used for BSE and DM. One particular model from [69] is shown here, which uses a geochemical BSE [60] and the relatively "warm" DM composition of [68], and results in the piles enriched by factors of 6.3 and 12 relative to the ambient mantle for U and Th, respectively. Some model combinations result in higher enrichments, and therefore a more pronounced variation of the geoneutrino signal. However, strong enrichment in radiogenic heat production has dynamical consequences on the stability and longevity of such piles and may work against the geochemical requirement of primordial nature of the enriched reservoir. This is an area of active research in geodynamics [86, 144, 145].

Figure 11 follows from Figures 8 and 10 and shows the fraction of the total signal (from crust + mantle, assuming no radioactivity in the core) that is coming from the mantle. It clearly shows the benefit of geoneutrino detection at an oceanic site in the Pacific ocean away from nuclear reactors, where the proportion of the signal from a mantle with geochemical BSE abundances can be as high at 80%. Pacific ocean basin as also the location of a mantle flux maximum is predicted from the thermochemical piles model. It is proposed that geoneutrino detection at two Pacific sites, one being at the predicted peak of mantle flux and the other away from it, may be exploited to test the chemical piles hypothesis [69].

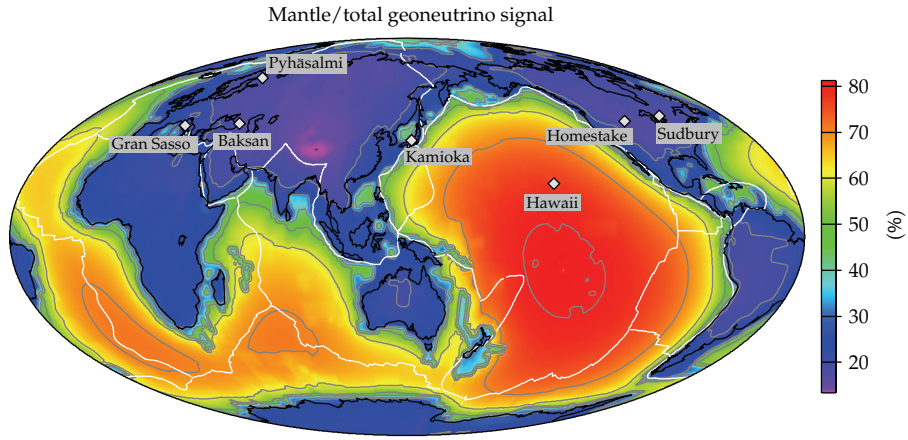


**Figure 11:** Ratio of mantle to total (mantle + crust) geoneutrino signal as predicted from crustal and mantle models shown in Figures 8 and 10. See [69].

## 9. Geoneutrino Observations

Geoneutrinos have been now observed at ~4$\sigma$ confidence level (CL) by both operating detectors: KamLAND and Borexino. Extracting geophysical information from geoneutrino measurements is not straightforward. The geoneutrino event rate prediction is obtained with an integration of the energy spectrum of antineutrino contributions coming from U and Th distributed in the Earth volume, weighted by the inverse square distance, subject to oscillations, and modulated by interaction cross-section ([146] and (6.5)).

### *9.1. KamLAND Measurement*

The first detection of geoneutrinos was reported by KamLAND group in 2005 [18]. It is based on detector live-time of 749.1 ± 0.5 days, (3.46 ± 0.17) × $10^{31}$ of target protons, that is, an exposure of (7.09 ± 0.35) × $10^{31}$ target proton years. The detector efficiency is estimated at 0.687 ± 0.007. Their maximum-likelihood analysis, constrained to Th/U ratio of 3.9, gives $28^{+16}_{-15}$ geoneutrino events. The corresponding flux is $6.4^{+3.6}_{-3.4}\,\mathrm{cm}^{-2}\,\mu\mathrm{s}^{-1}$. The 99% CL upper limit is 71 geoneutrino events or flux of $16.2\,\mathrm{cm}^{-2}\,\mu\mathrm{s}^{-1}$, which translates into a radiogenic power of 60 TW from $^{238}$U + $^{232}$Th (i.e., heat production that would exceed the Earth's heat loss).

Continued KamLAND measurement benefited from instrumentation improvements and decreased in nuclear reactor flux (shutdown of Kashiwazaki-Kariwa nuclear power plant following a 2007 earthquake). New results reported in 2011 [19] extend the previous data set. Data are based on exposure of (3.49 ± 0.07) × $10^{32}$ target proton years, or a live-time of 2135 days (5.8 years) and (5.98 ± 0.12) × $10^{31}$ target protons in the fiducial volume. Of the 841 candidate $\overline{\nu}_e$ events within the geoneutrino energy limits, 729 ± 32 is the predicted background, and $111^{+45}_{-43}$ were considered geoneutrino events. Maximum-likelihood analysis of the data, unconstrained with respect to Th/U ratio, gives 65 and 33 geoneutrino events from $^{238}$U and $^{232}$Th, respectively. This translates to Th/U ratio of 7.6 (6.13); however, Th/U remains unconstrained at 1$\sigma$ level. Constraining Th/U to 3.9 yields a total number of $106^{+29}_{-28}$ geoneutrino events, or a geoneutrino signal rate of 38 ± 10 TNU and heat production of $20^{+8.8}_{-8.6}$ TW from $^{238}$U + $^{232}$Th. Null hypothesis of no geoneutrinos is rejected at 99.997%

CL. KamLAND results also provide a 90% CL upper limit of 5.2 TW on the power of a hypothetical nuclear georeactor in the Earth's core. Assessment of KamLAND data by Dye [39] argues for a mantle signal rate of $12 \pm 11$ TNU at Kamioka.

### 9.2. Borexino Measurement

Borexino collaboration reported geoneutrino detection in 2010 [20]. Of the 15 candidate event in the geoneutrino energy window, $5.3 \pm 0.3$ constitute background. An unconstrained maximum-likelihood analysis yields $9.9^{+4.4}_{-3.4}$ geoneutrino events. Assuming Th/K = 3.9, this translates to a signal rate of $65^{+27}_{-22}$ TNU. A geoneutrino null hypothesis rejected at 99.997 CL. Borexino data give a 95% CL upper limit of 3 TW on the power of a nuclear georeactor in the core. This is a better constraint compared to one from KamLAND, a benefit of much lower man-made reactor $\overline{\nu}_e$ signal at Gran Sasso. According to Dye [39], Borexino registers a mantle geoneutrino signal at a rate of $40^{+27}_{-23}$ TNU at Gran Sasso.

### 9.3. Combined KamLAND + Borexino Analysis

A combined analysis of the KamLAND and Borexino data was performed by Fogli et al. [147] and most recently by Fiorentini et al. [146] with a focus on constraining the mantle component of the geoneutrino signal. In [146], the null hypothesis of no geoneutrino flux is rejected at $4.2\sigma$. After subtraction of crustal signal, based on a crustal reference model that includes local refinements, the mantle rate emerges at $2.4\sigma$ (98.4% CL) assuming that the mantle signal is identical at the two sites. The preferred value of Th/U ratio ~8 is not statistically significant, since any Th/U value is permissible at $1\sigma$ level. When Th/U is constrained to reflect variation between various BSE abundance estimates, $1.7 \leq \text{Th/U} \leq 3.9$, the analysis results in a mantle signal rate of $23 \pm 10$ TNU from $^{238}$U + $^{232}$Th [146]. Figure 12 shows the results in relation to various models of BSE composition.

## 10. Discussion and Prospects

Geologists already know that there is a lot of radioactivity in the continental crust (8 TW) and they know it quite well ($\pm 1$ TW). They are asking about the mantle: is it "cosmochemical" (so that it produces $3 \pm 2$ TW of radiogenic power), "geochemical" ($12 \pm 4$ TW), or "geodynamical" ($25 \pm 3$ TW)? Nondirectional geoneutrino detection at the existing and future continental sites cannot resolve mantle models, even with the improved precision of future detectors [39]. Oceanic deployment of a geoneutrino detector away from continental crust and nuclear power plants has been repeatedly suggested as a way to optimize the sensitivity to mantle signal [17, 19, 36, 38, 40]. It is proposed that an oceanic site detection in the Pacific can resolve the mantle models [39, 69].

### 10.1. $^{40}$K Geoneutrinos?

Potassium accounts for some 20% of radiogenic power within the Earth. Antineutrinos from potassium are produced entirely below the energy threshold of antineutrino quasielastic scattering on free protons, thus currently undetectable. Dye [39] discusses possibilities of $^{40}$K

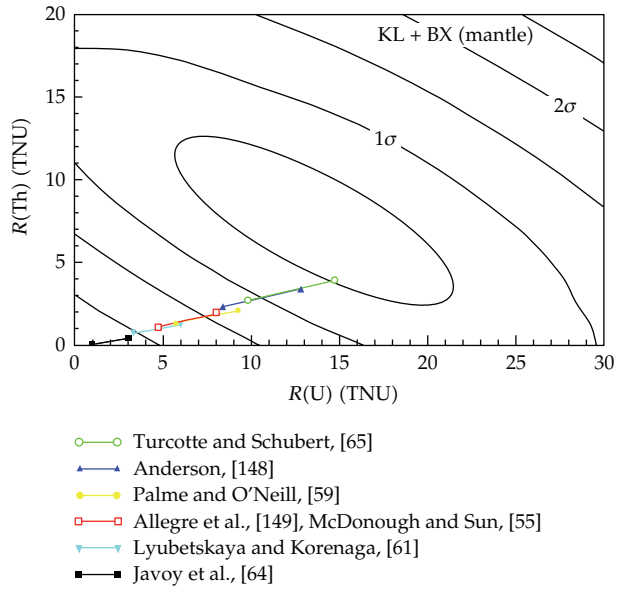


**Figure 12:** Experimental constraints on mantle flux from combined analysis of KamLAND and Borexino data (black contour lines), compared to predictions from various BSE abundance estimates [55, 59, 61, 64, 65, 148, 149]. Adapted from [146].

antineutrino detections, which include scattering on other nuclear targets ($^3$He or $^{106}$Cd) and elastic scattering on atomic electrons. Both methods require further development.

### *10.2. Directionality?*

The angular distribution of geoneutrinos was investigated in [38, 150–152] and most recently in [40]. Differences in angular distribution of geoneutrinos arriving from the crust and the mantle could be used to separate the signals if the directional information was available. Directional measurement away from continents might resolve a deep-seated mantle reservoir [40]. Directional detection was achieved in a statistical sense in the CHOOZ experiment, which uses a loaded liquid scintillator, by observing the weak correlation between the incident and the prompt-to-delayed-signal direction in inverse $\beta$-decay [153]. In principle, it is possible to exploit this correlation also for unloaded scintillators, such as those used in geoneutrino studies, however, obtaining statistically significant result requires thousands of events, well above the yield of geoneutrino detectors [154]. As we have noted earlier, electron (charged current) events below the inverse beta threshold will preserve neutrino directionality rather well. So, despite the more difficult extraction of these signatures from background (no delayed neutron tag) these events offer interesting potential for resolving source directions and ultimately geoneutrino Earth tomography.

## 11. Conclusion

We have reviewed the short history of geoneutrinos, the budding study of electron antineutrinos from inside the Earth as a unique telltale of the source of internal Earth heating.

While the notion of using the neutrinos from the uranium and thorium decay chains has been around for decades, notably stimulated by the landmark paper of Krauss et al. in 1984 [15], it is only in the last decade that the tiny geoneutrino interaction rate has begun to be revealed by the hundreds of tons KamLAND and Borexino experiments. The signals are feeble and we have barely reached five standard deviation detection, yet we are now less than a factor of two off from our predictions about the absolute source of Earth heating. In other words, there is no surprising new source of electron antineutrinos in the energy range of 1.8 to 3.6 MeV. And it is no surprise that a geoneutrino signal does exist, inescapably since we know the U/Th content of at least the top few hundred kilometers of the Earth and we now know neutrino properties fairly well.

At present, since both KamLAND and Borexino are located near continental plate margins, the neutrino flux is dominated by sources in the local (<500 km) crust. Unfortunately the count of neutrinos from the mantle, which is where we want to know the U/Th content, is so far only a minute fraction of the total. We have reviewed some extreme models as arise from differing approaches in geoscience, and we find that we cannot yet distinguish between models, though the cosmochemical model [64] and the extremes of the collisional erosion model [62] seem to be disfavored at the $2.5\sigma$ level.

Progress is on the horizon with the launch of the SNO+ experiment in Canada. There are proposals for several very large experiments, the fifty-kiloton LENA to be located in a mine in Finland, the deep ocean Hanohano in the deep Pacific, and a twenty-kiloton scale (not surely determined yet) Daya Bay II detector in China. All of these are at least five years out.

Beyond simple counting of neutrinos from a given location, there is much to be done. First of all, moving detectors to various deep ocean locations can begin to explore the lateral inhomogeneity of the U/Th distribution. There is much opportunity for discovery here, should the hot spots or peculiar areas such as the mid-Pacific Rise be associated with concentrations of U/Th. Moreover, though largely dismissed by geologists, there have been multiple suggestions of natural deep reactors either in the core (deemed by most experts as extremely unlikely) to accumulations near the CMB (not as difficult to imagine, but also deemed unlikely). Such discoveries would of course be revolutionary in geology and planetary studies; long shots, but huge payoff. In any event, simply finding evidence for the curious upwelling regions as due to increased U/Th content would be a great discovery and fundamental to geodynamics as we have discussed herein.

Large electron antineutrino detectors have multiple uses, and happily these are not exclusive. For example, a geoneutrino detector would ineluctably record a signal from a galactic supernova over a few seconds. Other types of extremely infrequent astrophysical phenomena (such as a burst of neutrinos associated with a GRB event), may also be recorded, without interference with geoneutrino mapping. Also depending upon placement, such detectors would inevitably contribute to worldwide monitoring of reactors and for clandestine nuclear weapons testing. Some elementary particle studies can also be carried out, particularly with respect to the mass hierarchy and neutrino mixing angles. As well, there are possible experiments to be carried out with higher energy neutrinos, including those in the GeV energy range from a distant particle accelerator. The point, for this paper, is that there is a large physics and astrophysics community which is interested in collaborating in the geoneutrino venture, providing scientific stimulus, dissertation topics, and possibly cooperative funding opportunities. It is reasonable to expect large geoneutrino detectors to provide a cornucopia of scientific data.

On the experimental side, there is much to be improved upon over present-day instruments. Large and cost-effective detectors, particularly mobile (deep ocean) instruments are sought. New technology in doping of water for cost-effective light emission in huge volumes (needed as one gets to the 100-kiloton scale), new flat panel twenty-first-century light detectors, and advances in electronics (high-speed waveform digitizing, along with low-power and inexpensive channel costs), are under development. Some novel methods of inverse beta event imaging are being developed (miniTimeCube [128]). And there is ongoing work studying how to improve neutrino direction resolution, inverse beta tagging (time delay in positron annihilation), and seeking a means to (cost effectively) detect neutrinos from $^{40}$K decays. A study by a team from the University of Hawaii and the National Geospatial Agency has determined that remote nuclear reactor monitoring is indeed possible and have christened their techniques as NUDAR (NeUtrino Direction And Ranging) [155]. For point source recording, the neutrinos from a reactor carry not only direction but also range information due to the neutrino oscillation distorted spectrum. This group has shown that neutrino oscillations provide surprising ability to determine range given as few as hundreds of counts attributable to a given point source (unlike radar, NUDAR needs no active pinging of the target, but waits for a signal from the target). The relevance of this work to geoneutrinos is still being investigated, but one immediately sees the potential, even though oscillation signatures are smeared out due to distributed sources. This opens the door in the future, however, to real Earth tomography.

We expect the study of electron antineutrinos from the Earth to blossom into a rich cross disciplinary field, cutting across traditional boundaries and for which we predict a bright and exciting future.

## Acknowledgments

This paper benefited from reviews by two anonymous reviewers. The authors gratefully acknowledge support for this research from NSF EAR 0855791 CSEDI Collaborative Research: Neutrino Geophysics: Collaboration between Geology and Particle Physics.

## References

[1] W. Hopkins, "Preliminary observations on the refrigeration of the globe," *Philosophical Transactions of the Royal Society of London*, vol. 129, pp. 381–385, 1839.

[2] D. J. Stevenson, "Earth formation and evolution," in *Evolution of the Earth*, D. J. Stevenson, Ed., vol. 9 of *Treatise on Geophysics*, chapter 9.01, p. 111, Elsevier Scientific Publishing Company, New York, NY, USA, 2007, Editor-in-chief G. Schubert.

[3] W. Thomson, "On the secular cooling of the Earth," *Philosophical Magazine Series 4*, vol. 25, no. 165, pp. 1–14, 1863.

[4] L. Kelvin, "The age of the earth as an abode fitted for life," Annual Report of the Smithsonian Institution, 1897.

[5] J. D. Burchfield, *Lord Kelvin and the Age of the Earth*, Science History Publications, New York, NY, USA, 1975.

[6] G. B. Dalrymple, *The Age of the Earth*, Stanford University Press, Stanford, Calif, USA, 1991.

[7] E. Rutherford, *Radio-Activity*, Cambridge Physical Series, University Press, Cambridge, UK, 2nd edition, 1905.

[8] G. F. Davies, "Thermal evolution of the mantle," in *Evolution of the Earth*, D. J. Stevenson, Ed., vol. 9 of *Treatise on Geophysics*, chapter 9.08, pp. 197–216, Elsevier Scientific Publishing Company, New York, NY, USA, 2007, Editor-in-chief G. Schubert.

[9] N. H. Sleep, "Plate tectonics through time," in *Evolution of the Earth*, D. J. Stevenson, Ed., vol. 9 of *Treatise on Geophysics*, chapter 9.06, pp. 145–169, Elsevier Scientific Publishing Company, New York, NY, USA, 2007, Editor-in-chief G. Schubert.
[10] C. L. Cowan, F. Reines, F. B. Harrison, H. W. Kruse, and A. D. McGuire, "Detection of the free neutrino: a confirmation," *Science*, vol. 124, no. 3212, pp. 103–104, 1956.
[11] G. Eder, "Terrestrial neutrinos," *Nuclear Physics*, vol. 78, no. 3, pp. 657–662, 1966.
[12] G. Marx, "Geophysics by neutrinos," *Czechoslovak Journal of Physics B*, vol. 19, no. 12, pp. 1471–1479, 1969.
[13] G. Marx and I. Lux, "Hunting for soft antineutrinos," *Acta Physica Academiae Scientiarum Hungaricae*, vol. 28, no. 1–3, pp. 63–70, 1970.
[14] C. Avilez, G. Marx, and B. Fuentes, "Earth as a source of antineutrinos," *Physical Review D*, vol. 23, no. 5, pp. 1116–1117, 1981.
[15] L. M. Krauss, S. L. Glashow, and D. N. Schramm, "Antineutrino astronomy and geophysics," *Nature*, vol. 310, no. 5974, pp. 191–198, 1984.
[16] R. S. Raghavan, S. Schoenert, S. Enomoto, J. Shirai, F. Suekane, and A. Suzuki, "Measuring the global radioactivity in the earth by multidetector antineutrino spectroscopy," *Physical Review Letters*, vol. 80, no. 3, pp. 635–638, 1998.
[17] C. G. Rothschild, M. C. Chen, and F. P. Calaprice, "Antineutrino geophysics with liquid scintillator detectors," *Geophysical Research Letters*, vol. 25, no. 7, pp. 1083–1086, 1998.
[18] T. Araki, S. Enomoto, K. Furuno et al., "Experimental investigation of geologically produced antineutrinos with KamLAND," *Nature*, vol. 436, no. 7050, pp. 499–503, 2005.
[19] A. Gando, Y. Gando, K. Ichimura et al., "Partial radiogenic heat model for Earth revealed by geoneutrino measurements," *Nature Geoscience*, vol. 4, no. 9, pp. 647–651, 2011.
[20] G. Bellini, J. Benzigerm, S. Bonettih et al., "Observation of geo-neutrinos," *Physics Letters B*, vol. 687, no. 4-5, pp. 4299–5304, 2010.
[21] M. C. Chen, "Geo-neutrinos in SNO+," *Earth, Moon and Planets*, vol. 99, no. 1–4, pp. 221–228, 2006.
[22] M. Kobayashi and Y. Fukao, "The Earth as an antineutrino star," *Geophysical Research Letters*, vol. 18, no. 4, pp. 633–636, 1991.
[23] Neutrino Sciences 2005, Neutrino Geophysics, Honolulu, Hawaii, USA, December 2005, http://www.phys.hawaii.edu/~sdye/hnsc.html.
[24] Neutrino Sciences 2007, Deep Ocean Anti-Neutrino Observatory Workshop, Honolulu, Hawaii, USA, March 2007, http://www.phys.hawaii.edu/~sdye/hano.html.
[25] Neutrino Geoscience 2008 at SNOLAB, Sudbury, Ontario, Canada, September 2008, http://geonu.snolab.ca.
[26] Neutrino Geoscience 2010 at Gran Sasso National Laboratory—Italy, October, 2010, http://geoscience.lngs.infn.it/.
[27] Neutrino Geoscience Workshop, Deadwood, South Dakota, June 2011, http://www.dsu.edu/research/CETUP/2011.html.
[28] Geoneutrinos: A new tool for the study of the solid Earth I, Session U41F at AGU 2006 Joint Assembly, Baltimore, Md, USA, May 25, 2006.
[29] S. T. Dye, Ed., *Neutrino Geophysics: Proceedings of Neutrino Sciences 2005*, Springer, Dordrecht, The Netherlands, 2007.
[30] C. Lan, *SNO+ and geoneutrino physics [M.S. thesis]*, Queen's University, Kingston, Ontario, Canada, 2007.
[31] S. Enomoto, *Neutrino geophysics and observation of geo-neutrinos at KamLAND [Ph.D. thesis]*, Tohoku University, 2005.
[32] W. F. McDonough, "Geophysics: mapping the Earth's engine," *Science*, vol. 317, no. 5842, pp. 1177–1178, 2007.
[33] S. T. Dye, W. F. McDonough, and J. Mahoney, "Geoneutrino measurements and models investigate deep Earth," *Eos*, vol. 89, no. 44, pp. 433–434, 2008.
[34] W. F. McDonough, J. G. Learned, and S. T. Dye, "The many uses of electron antineutrinos," *Physics Today*, vol. 65, no. 3, pp. 46–51, 2012.
[35] A. Ananthaswamy, "Messengers from the underworld," *New Scientist*, vol. 214, no. 2862, pp. 32–35, 2012.
[36] S. Enomoto, E. Ohtani, K. Inoue, and A. Suzuki, "Neutrino geophysics with KamLAND and future prospects," *Earth and Planetary Science Letters*, vol. 258, no. 1-2, pp. 147–159, 2007.
[37] G. Fiorentini, M. Lissia, and F. Mantovani, "Geo-neutrinos and earth's interior," *Physics Reports*, vol. 453, no. 5-6, pp. 117–172, 2007.

[38] S. T. Dye, "Geo-neutrinos and silicate earth enrichment of U and Th," *Earth and Planetary Science Letters*, vol. 297, no. 1-2, pp. 1–9, 2010.
[39] S. T. Dye, "Geoneutrinos and the radioactive power of the Earth," *Reviews of Geophysics*, vol. 50, no. 3, Article ID RG3007, 2012.
[40] J.-C. Mareschal, C. Jaupart, C. Phaneuf, and C. Perry, "Geoneutrinos and the energy budget of the Earth," *Journal of Geodynamics*, vol. 54, pp. 43–54, 2012.
[41] C. Jaupart, S. Labrosse, and J. C. Mareschal, "Temperatures, heat and energy in the mantle of the Earth," in *Mantle Dynamics*, D. Bercovici, Ed., vol. 7 of *Treatise on Geophysics*, chapter 7.06, pp. 253–303, Elsevier Scientific Publishing Company, New York, NY, USA, 2007, editor-in-chief G. Schubert.
[42] J. Korenaga, "Urey ratio and the structure and evolution of Earth's mantle," *Reviews of Geophysics*, vol. 46, no. 2, Article ID RG2007, 2008.
[43] T. Lay, J. Hernlund, and B. A. Buffett, "Core-mantle boundary heat flow," *Nature Geoscience*, vol. 1, no. 1, pp. 25–32, 2008.
[44] J. G. Sclater, C. Jaupart, and D. Galson, "The heat flow through oceanic and continental crust and the heat loss of the earth," *Reviews of Geophysics and Space Physics*, vol. 18, no. 1, pp. 269–311, 1980.
[45] G. F. Davies, "Review of oceanic and global heat flow estimates," *Reviews of Geophysics*, vol. 18, no. 3, pp. 718–722, 1980.
[46] H. N. Pollack, S. J. Hurter, and J. R. Johnson, "Heat flow from the Earth's interior: analysis of the global data set," *Reviews of Geophysics*, vol. 31, no. 3, pp. 267–280,, 1993.
[47] J. H. Davies and D. R. Davies, "Earth's surface heat flux," *Solid Earth*, vol. 1, no. 1, pp. 5–24, 2010.
[48] C. A. Stein and S. Stein, "A model for the global variation in oceanic depth and heat flow with lithospheric age," *Nature*, vol. 359, no. 6391, pp. 123–129, 1992.
[49] A. M. Hofmeister and R. E. Criss, "Earth's heat flux revised and linked to chemistry," *Tectonophysics*, vol. 395, no. 3-4, pp. 159–177, 2005.
[50] R. Von Herzen, E. E. Davis, A. T. Fisher, C. A. Stein, and H. N. Pollack, "Comments on "Earth's heat flux revised and linked to chemistry" by A.M. Hofmeister and R.E. Criss," *Tectonophysics*, vol. 409, no. 1–4, pp. 193–198, 2005.
[51] M. Wei and D. Sandwell, "Estimates of heat flow from Cenozoic seafloor using global depth and age data," *Tectonophysics*, vol. 417, no. 3-4, pp. 325–335, 2006.
[52] T. W. Becker, C. P. Conrad, B. Buffett, and R. D. M. Müller, "Past and present sea floor age distributions and the temporal evolution of plate tectonic heat transport," *Earth and Planetary Science Letters*, vol. 278, no. 3-4, pp. 233–242, 2009.
[53] R. L. Rudnick and S. Gao, "Composition of the continental crust," in *The Crust*, R. L. Rudnick, Ed., vol. 3 of *Treatise on Geochemistry*, chapter 3.01, pp. 10–6408, Elsevier Scientific Publishing Company, Oxford, UK, 2003, Editors-in-chief H. D. Holland and K. K. Turekian.
[54] F. Nimmo, "Energetics of the core," in *Core Dynamics*, P. Olson, Ed., vol. 8 of *Treatise on Geophysics*, chapter 8.02, pp. 31–65, Elsevier Scientific Publishing Company, New York, NY, USA, 2007.
[55] W. F. McDonough and S. Sun, "The composition of the Earth," *Chemical Geology*, vol. 120, no. 3- 4, pp. 223–253, 1995.
[56] G. J. Wasserburg, G. J. F. Macdonald, F. Hoyle, and W. A. Fowler, "Relative contributions of uranium, thorium, and potassium to heat production in the earth," *Science*, vol. 143, no. 3605, pp. 465–467, 1964.
[57] W. F. McDonough, "Compositional model for the Earth's core," in *The Mantle and Core, Treatise on Geochemistry*, R. W. Carlson, Ed., vol. 2, chapter 2.15, pp. 547–568, Elsevier Scientific Publishing Company, Oxford, UK, 2003, Editors-in-chief H. D. Holland and K. K. Turekian.
[58] S. R. Hart and A. Zindler, "In search of a bulk-Earth composition," *Chemical Geology*, vol. 57, no. 34, pp. 247–267, 1986.
[59] H. Palme and H. S. C. O'Neill, "Cosmochemical estimates of mantle composition," in *Treatise on Geochemistry*, R. W. Carlson, Ed., vol. 2, chapter 2.01, pp. 1380–1308, Elsevier Scientific Publishing Company, Oxford, UK, 2003, Editors-in-chief H. D. Holland and K. K. Turekian.
[60] R. Arevalo Jr., W. F. McDonough, and M. Luong, "The K/U ratio of the silicate Earth: insights into mantle composition, structure and thermal evolution," *Earth and Planetary Science Letters*, vol. 278, no. 3-4, pp. 361–369, 2009.
[61] T. Lyubetskaya and J. Korenaga, "Chemical composition of Earth's primitive mantle and its variance: 1. Method and results," *Journal of Geophysical Research B*, vol. 112, no. 3, Article ID B03211, 2007.
[62] H. S. C. O'Neill and H. Palme, "Collisional erosion and the non-chondritic composition of the terrestrial planets," *Philosophical Transactions of the Royal Society A*, vol. 366, no. 1883, pp. 4205–4238, 2008.

[63] M. Javoy, "Chemical Earth models," *Comptes Rendus de l'Académie des Sciences*, vol. 329, no. 8, pp. 537–555, 1999.

[64] M. Javoy, E. Kaminski, F. Guyot et al., "The chemical composition of the Earth: enstatite chondrite models," *Earth and Planetary Science Letters*, vol. 293, no. 3-4, pp. 259–268, 2010.

[65] D. L. Turcotte, G. Schubert, and Geodynamics, *Applications of Continuum Physics to Geological Problems*, Cambridge University Press, 2nd edition, 2002.

[66] R. K. Workman and S. R. Hart, "Major and trace element composition of the depleted MORB mantle (DMM)," *Earth and Planetary Science Letters*, vol. 231, no. 1-2, pp. 53–72, 2005.

[67] V. J. M. Salters and A. Stracke, "Composition of the depleted mantle," *Geochemistry, Geophysics, Geosystems*, vol. 5, no. 5, Article ID Q05B07, 27 pages, 2004.

[68] R. Arevalo Jr. and W. F. McDonough, "Chemical variations and regional diversity observed in MORB," *Chemical Geology*, vol. 271, no. 1-2, pp. 70–85, 2010.

[69] O. Šrámek, W. F. McDonough, E. S. Kite, V. Lekić, S. T. Dye, and S. Zhong, "Geophysical and geochemical constraints on geoneutrino fluxes from Earth's mantle," *Earth and Planetary Science Letters*.

[70] G. Schubert, D. L. Turcotte, and P. Olson, *Mantle Convection in Earth and Planets*, Cambridge University Press, Cambridge, UK, 2001.

[71] D. Bercovici, "Mantle dynamics past, present and future: an introduction and overview," in *Mantle Dynamics, Treatise on Geo-physics*, D. Bercovici, Ed., vol. 7, chapter 7.01, p. 130, Elsevier Scientific Publishing Company, New York, NY, USA, 2007, Editor-in-chief G. Schubert.

[72] G. F. Davies, *Dynamic Earth: Plates, Plumes and Mantle Convection*, Cambridge University Press, 1999.

[73] U. Christensen, "Thermal evolution models for the Earth," *Journal of Geophysical Research*, vol. 90, no. 4, pp. 2995–3007, 1985.

[74] J. Korenaga, "Archean geodynamics and the thermal evolution of earth," in *Archean Geodynamics and Environments*, K. Benn, J. C. Mareschal, and K. Condie, Eds., vol. 164 of *AGU Geophysical Monograph*, p. 732, American Geophysical Union, 2006.

[75] G. F. Davies, "Effect of plate bending on the Urey ratio and the thermal evolution of the mantle," *Earth and Planetary Science Letters*, vol. 287, no. 3-4, pp. 513–518, 2009.

[76] S. Labrosse and C. Jaupart, "Thermal evolution of the Earth: secular changes and uctuations of plate characteristics," *Earth and Planetary Science Letters*, vol. 260, no. 3-4, pp. 465–481, 2007.

[77] P. G. Silver and M. D. Behn, "Intermittent plate tectonics," *Science*, vol. 319, no. 5859, pp. 85–88, 2008.

[78] A. Lenardic, C. M. Cooper, and L. Moresi, "A note on continents and the Earth's Urey ratio," *Physics of the Earth and Planetary Interiors*, vol. 188, no. 1-2, pp. 127–130, 2011.

[79] J. W. Crowley, M. Gérault, and R. J. O'Connell, "On the relative in uence of heat and water transport on planetary dynamics," *Earth and Planetary Science Letters*, vol. 310, no. 34, pp. 380–388, 2011.

[80] T. Nakagawa and P. J. Tackley, "Influence of magmatism on mantle cooling, surface heat flow and Urey ratio," *Earth and Planetary Science Letters*, vol. 329-330, pp. 1–10, 2012.

[81] A. W. Hofmann, "Mantle geochemistry: the message from oceanic volcanism," *Nature*, vol. 385, no. 6613, pp. 219–229, 1997.

[82] R. D. van der Hilst, S. Widiyantoro, and E. R. Engdahl, "Evidence for deep mantle circulation from global tomography," *Nature*, vol. 386, no. 6625, pp. 578–584, 1997.

[83] Y. Fukao, S. Widiyantoro, and M. Obayashi, "Stagnant slabs in the upper and lower mantle transition region," *Reviews of Geophysics*, vol. 39, no. 3, pp. 291–323, 2001.

[84] T. Lay, Q. Williams, and E. J. Garnero, "The core-mantle boundary layer and deep Earth dynamics," *Nature*, vol. 392, no. 6675, pp. 461–468, 1998.

[85] E. J. Garnero and A. K. McNamara, "Structure and dynamics of Earth's lower mantle," *Science*, vol. 320, no. 5876, pp. 626–628, 2008.

[86] A. K. McNamara, E. J. Garnero, and S. Rost, "Tracking deep mantle reservoirs with ultra-low velocity zones," *Earth and Planetary Science Letters*, vol. 299, no. 1-2, pp. 1–9, 2010.

[87] L. Wen, P. Silver, D. James, and R. Kuehnel, "Seismic evidence for a thermo-chemical boundary at the base of the Earth's mantle," *Earth and Planetary Science Letters*, vol. 189, no. 3-4, pp. 141–153, 2001.

[88] W.-J. Su and A. M. Dziewonski, "Simultaneous inversion for 3-D variations in shear and bulk velocity in the mantle," *Physics of the Earth and Planetary Interiors*, vol. 100, no. 1–4, pp. 135–156, 1997.

[89] M. J. Walter and R. G. Tronnes, "Early Earth dierentiation," *Earth and Planetary Science Letters*, vol. 225, no. 3-4, pp. 253–269, 2004.

[90] C.-T. A. Lee, Q. Z. Yin, A. Lenardic, A. Agranier, C. J. O'Neill, and N. Thiagarajan, "Trace-element composition of Fe-rich residual liquids formed by fractional crystallization: implications for the Hadean magma ocean," *Geochimica et Cosmochimica Acta*, vol. 71, no. 14, pp. 3601–3615, 2007.

[91] V. C. Bennett, A. D. Brandon, and A. P. Nutman, "Coupled $^{142}$Nd-$^{143}$Nd isotopic evidence for Hadean mantle dynamics," *Science*, vol. 318, no. 5858, pp. 1907–1910, 2007.

[92] S. Labrosse, J. W. Hernlund, and N. Coltice, "A crystallizing dense magma ocean at the base of the Earth's mantle," *Nature*, vol. 450, no. 7171, pp. 866–869, 2007.

[93] J. Ritsema, H. J. van Heijst, and J. H. Woodhouse, "Complex shear wave velocity structure imaged beneath Africa and Iceland," *Science*, vol. 286, no. 5446, pp. 1925–1928, 1999.

[94] J. Ritsema, H. J. van Heijst, and J. H. Woodhouse, "Global transition zone tomography," *Journal Of Geophysical Research*, vol. 109, Article ID B02302, 14 pages, 2004.

[95] A. L. Bull, A. K. McNamara, and J. Ritsema, "Synthetic tomography of plume clusters and thermochemical piles," *Earth and Planetary Science Letters*, vol. 278, no. 3-4, pp. 152–162, 2009.

[96] M. G. Jackson and R. W. Carlson, "An ancient recipe for ood-basalt genesis," *Nature*, vol. 476, pp. 316–319, 2011.

[97] M. Willbold, T. Elliott, and S. Moorbath, "The tungsten isotopic composition of the Earth's mantle before the terminal bombardment," *Nature*, vol. 477, no. 7363, pp. 195–198, 2011.

[98] P. H. Warren, "Stable-isotopic anomalies and the accretionary assemblage of the Earth and Mars: A subordinate role for carbonaceous chondrites," *Earth and Planetary Science Letters*, vol. 311, no. 1-2, pp. 93–100, 2011.

[99] C. Fitoussi and B. Bourdon, "Silicon isotope evidence against an enstatite chondrite Earth," *Science*, vol. 335, no. 6075, pp. 1477–1480, 2012.

[100] I. H. Campbell and H. St. C. O'Neill, "Evidence against a chondritic Earth," *Nature*, vol. 483, no. 7391, pp. 553–558, 2012.

[101] J. Zhang, N. Dauphas, A. M. Davis, I. Leya, and A. Fedkin, "The proto-Earth as a significant source of lunar material," *Nature Geoscience*, vol. 5, no. 4, pp. 251–255, 2012.

[102] M. Murakami, Y. Ohishi, N. Hirao, and K. Hirose, "A perovskitic lower mantle inferred from high-pressure, high-temperature sound velocity data," *Nature*, vol. 485, no. 7396, pp. 90–94, 2012.

[103] D. Abbott, L. Burgess, J. Longhi, and W. H. F. Smith, "An empirical thermal history of the Earth's upper mantle," *Journal of Geophysical Research*, vol. 99, no. 7, pp. 13835–13850, 1994.

[104] W. F. McDonough and R. Arevalo Jr., "Uncertainties in the composition of Earth, its core and silicate sphere," *Journal of Physics: Conference Series*, vol. 136, no. 2, Article ID 022006, 2008.

[105] C. K. Gessmann and B. J. Wood, "Potassium in the Earth's core?" *Earth and Planetary Science Letters*, vol. 200, no. 1-2, pp. 63–78, 2002.

[106] V. R. Murthy, W. van Westrenen, and Y. Fei, "Experimental evidence that potassium is a substantial radioactive heat source in planetary cores," *Nature*, vol. 423, no. 6936, pp. 163–165, 2003.

[107] V. R. Murthy, "Radioactivity of the Earth and the case for potassium in the Earth's core," *Earth, Moon, Planets*, vol. 99, no. 1, pp. 23–32, 2006.

[108] J. M. Herndon, "Substructure of the inner core of the Earth," *Proceedings of the National Academy of Sciences*, vol. 93, no. 2, pp. 646–648, 1996.

[109] J. R. Lancelot, A. Vitrac, and C. J. Allegre, "The Oklo natural reactor: age and evolution studies by U—Pb and Rb—Sr systematics," *Earth and Planetary Science Letters*, vol. 25, no. 2, pp. 189–196, 1975.

[110] R. J. D. Meijer and W. van Westrenen, "The feasibility and implications of nuclear georeactors in Earth's core-mantle boundary region," *South African Journal of Science*, vol. 104, no. 3-4, pp. 111–118, 2008.

[111] J. M. Herndon, "Nuclear georeactor origin of oceanic basalt $^{3}$He/$^{4}$He, evidence, and implications," *Proceedings of the National Academy of Sciences*, vol. 100, no. 6, pp. 3047–3050, 2003.

[112] G. Audi and A. Wapstra, "The update to the atomic mass evaluation," *Nuclear Physics A*, vol. 595, no. 4, pp. 409–480, 1995.

[113] R. B. Firestone and V. S. Shirley, *Table of Isotopes*, John Wiley & Sons, New York, NY, USA, 8th edition, 1996.

[114] G. Fiorentini, A. Ianni, G. Korga et al., "Nuclear physics for geo-neutrino studies," *Physical Review C*, vol. 81, no. 3, Article ID 034602, 9 pages, 2010.

[115] B. Pontecorvo, "Mesonium and antimesonium," *Soviet Journal of Experimental and Theoretical Physics*, vol. 6, no. 2, pp. 429–431, 1958.

[116] G. L. Fogli, E. Lisi, A. Marrone, A. Palazzo, and A. M. Rotunno, "Evidence of $\theta_{13} > 0$ from global neutrino data analysis," *Physical Review D*, vol. 84, no. 5, Article ID 053007, 7 pages, 2011.

[117] The Daya Bay Collaboration, "Observation of electron-antineutrino disappearance at Daya Bay," *Physical Review Letters*, vol. 108, no. 17, Article ID 171803, 2012.

[118] RENO Collaboration, "Observation of reactor electron antineutrinos disappearance in the RENO experiment," *Physical Review Letters*, vol. 108, no. 19, Article ID 191802, 2012.

[119] K. Nakamura and P. D. Group, "Review of particle physics," *Journal of Physics G*, vol. 37, no. 7, Article ID 075021, 2010.

[120] C. L. Cowan, F. Reines, F. B. Harrison, E. C. Anderson, and F. N. Hayes, "Large liquid scintillation detectors," *Physical Review*, vol. 90, no. 3, pp. 493–494, 1953.

[121] F. Reines and C. L. Cowan, "A proposed experiment to detect the free neutrino," *Physical Review*, vol. 90, no. 3, pp. 492–493, 1953.

[122] J. Learned, S. Dye, and S. Pakvasa, "Neutrino geophysics conference introduction," *Earth, Moon, Planets*, vol. 99, no. 1, pp. 1–15, 2006.

[123] P. Vogel and J. F. Beacom, "Angular distribution of neutron inverse beta decay, $\overline{v}_e + p \rightarrow e^+ + n$," *Physical Review D*, vol. 60, no. 5, Article ID 053003, 1999.

[124] F. Mantovani, L. Carmignani, G. Fiorentini, and M. Lissia, "Antineutrinos from Earth: a reference model and its uncertainties," *Physical Review D*, vol. 69, no. 1, Article ID 013001, 2004.

[125] A. M. Dziewonski and D. L. Anderson, "Preliminary reference Earth model," *Physics of the Earth and Planetary Interiors*, vol. 25, no. 4, pp. 297–356, 1981.

[126] C. Bassin, G. Laske, and G. Masters, "The current limits of resolution for surface wave tomography in North America," *Eos, Transactions, American Geophysical Union*, vol. 81, no. 48, p. F897, 2000, http://igppweb.ucsd.edu/~gabi/crust2.html.

[127] F. Reines, H. S. Gurr, and H. W. Sobel, "Detection of $\overline{v}_e - e$ scattering," *Physical Review Letters*, vol. 37, no. 6, pp. 315–318, 1976.

[128] J. G. Learned, "The mini-Time-Cube—A portable directional anti-neutrino detector," presentation at Advances in Neutrino Technology 2011, Philadephia, Pa, USA, 2011.

[129] G. Alimonti, C. Arpesella, H. Back et al., "The Borexino detector at the Laboratori Nazionali del Gran Sasso," *Nuclear Instruments and Methods in Physics*, vol. 600, no. 3, pp. 568–593, 2009.

[130] M. Wurm, J. F. Beacomc, L. B. Bezrukovd et al., "The next-generation liquid-scintillator neutrino observatory LENA," *Astroparticle Physics*, vol. 35, no. 11, pp. 685–732, 2012.

[131] N. Tolich, Y.-D. Chan, C. A. Currat et al., "A geoneutrino experiment at Homestake," *Earth, Moon, Planets*, vol. 99, no. 1, pp. 229–240, 2006.

[132] I. R. Barabanov, G. Y. Novikova, V. V. Sinev, and E. A. Yanovich, "Research of the natural neutrino uxes by use of large volume scintillation detector at Baksan," http://arxiv.org/abs/0908.1466.

[133] S. Dye, E. Guillian, J. G. Learned et al., "Earth radioactivity measurements with a deep ocean anti-neutrino observatory," *Earth, Moon, Planets*, vol. 99, no. 1–4, pp. 241–252, 2006.

[134] J. G. Learned, S. T. Dye, and S. Pakvasa, "Hanohano: a deep ocean anti-neutrino detector for unique neutrino physics and geophysics studies," in *Proceedings of the 12th International Workshop on Neutrino Telescopes*, Venice, Italy, March 2007.

[135] Y. Wang, "Daya Bay experiment and its future," presentation at XIV International Workshop on Neutrino Telescopes, Venice, Italy, March 2011, http://neutrino.pd.infn.it/Neutel2011/.

[136] G. Fiorentini, M. Lissia, F. Mantovani, and R. Vannucci, "How much uranium is in the Earth? Predictions for geoneutrinos at KamLAND," *Physical Review D*, vol. 72, no. 3, Article ID 033017, 2005.

[137] G. Fiorentini, M. Lissia, F. Mantovani, and R. Vannucci, "Geo-neutrinos: a new probe of Earth's interior," *Earth and Planetary Science Letters*, vol. 238, no. 1-2, pp. 235–247, 2005.

[138] K. A. Hochmuth, F. V. Feilitzsch, B. D. Fields et al., "Probing the Earth's interior with a large volume liquid scintillator detector," *Astroparticle Physics*, vol. 27, no. 1, pp. 21–29, 2007.

[139] E. S. Kite and V. Lekic, "Feasibility of mantle radiogenic power determination with geoneutrinos," unpublished.

[140] M. Coltorti, R. Borasoa, F. Mantovani et al., "U and Th content in the Central Apennines continental crust: a contribution to the determination of the geo-neutrinos ux at LNGS," *Geochimica et Cosmochimica Acta*, vol. 75, no. 9, pp. 2271–2294, 2011.

[141] W. M. White and E. M. Klein, "The oceanic crust," in *The Crust*, R. L. Rudnick, Ed., vol. 3 of *Treatise on Geochemistry*, chapter 14, Elsevier Scientific Publishing Company, Oxford, UK, 2nd edition, 2013, editors-in-chief H. D. Holland and K. K. Turekian.

[142] T. Plank, "The oceanic crust," in *The Crust*, R. L. Rudnick, Ed., vol. 3 of *Treatise on Geochemistry*, Elsevier Scientific Publishing Company, Oxford, UK, 2nd edition, 2013, editors-in-chief H. D. Holland and K. K. Turekian.

[143] Y. Huang, V. Chubakov, F. Mantovani, W. F. McDonough, and R. L. Rudnick, "A reference Earth model for the heat producing elements and associated geoneutrino flux," submitted to *Geochemistry, Geophysics, Geosystems*.

[144] F. Deschamps, E. Kaminski, and P. J. Tackley, "A deep mantle origin for the primitive signature of ocean island basalt," *Nature Geoscience*, vol. 4, no. 12, pp. 879–882, 2011.

[145] P. J. Tackley, "Dynamics and evolution of the deep mantle resulting from thermal, chemical, phase and melting effects," *Earth-Science Reviews*, vol. 110, no. 1–4, pp. 1–25, 2012.

[146] G. Fiorentini, G. L. Fogli, E. Lisi, F. Mantovani, and A. M. Rotunno, "Mantle geoneutrinos in KamLAND and Borexino," *Physical Review D*, vol. 86, no. 3, Article ID 033004, 2012.

[147] G. L. Fogli, E. Lisi, A. Palazzo, and A. M. Rotunno, "Combined analysis of KamLAND and Borexino neutrino signals from Th and U decays in the Earth's interior," *Physical Review D*, vol. 82, no. 9, Article ID 093006, 2010.

[148] D. L. Anderson, *The New Theory of the Earth*, Cambridge University Press, 2007.

[149] C. J. Allègre, J. P. Poirier, E. Humler, and A. W. Hofmann, "The chemical composition of the Earth," *Earth and Planetary Science Letters*, vol. 134, no. 3-4, pp. 515–526, 1995.

[150] B. Fields and K. Hochmuth, "Imaging the Earth's interior: the angular distribution of terrestrial neutrinos," *Earth, Moon, Planets*, vol. 99, no. 1, pp. 155–181, 2006.

[151] A. Suzuki, "Physics in next geoneutrino detectors," *Earth, Moon, Planets*, vol. 99, no. 1, pp. 359–368, 2006.

[152] K. A. Hochmuth, "The angular distribution of geoneutrinos," *Progress in Particle and Nuclear Physics*, vol. 57, no. 1, pp. 293–295, 2006.

[153] M. Apollonio, A. Baldini, C. Bemporad et al., "Determination of neutrino incoming direction in the CHOOZ experiment and its application to supernova explosion location by scintillator detectors," *Physical Review D*, vol. 61, no. 1, Article ID 012001, 1999.

[154] M. Batygov, "On the possibility of directional analysis for geo-neutrinos," *Earth, Moon, Planets*, vol. 99, no. 1, pp. 183–192, 2006.

[155] G. R. Jocher, D. A. Bondy, B. M. Dobbs et al., "Theoretical antineutrino detection, direction and ranging at long distances," *Physics Reports*. In press.